

N 7 1 - 3 4 3 6 2

NASA CR 121659

ATS-03061

EXPLORER XXXI  
ION MASS SPECTROMETER EXPERIMENT

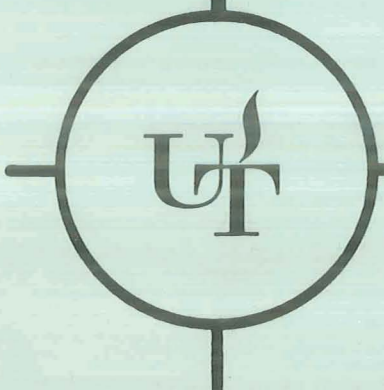
CASE FILE  
COPY

FINAL REPORT

NASA CONTRACTS

NAS 5-9444 AND NSR 44-004-089

25 JULY 1971



THE UNIVERSITY OF TEXAS AT DALLAS

POST OFFICE BOX 30365

DALLAS, TEXAS 75230

THE UNIVERSITY OF TEXAS AT DALLAS  
DALLAS, TEXAS

25 July 1971

EXPLORER XXXI  
ION MASS SPECTROMETER EXPERIMENT  
FINAL REPORT


NASA CONTRACTS  
NAS 5-9444 and NSR 44-004-089

Prepared by:



William P. Lord  
Research Engineer  
Associate

Approved by:



John H. Hoffman  
Principal Investigator

## CONTENTS

### SECTION 1 - INTRODUCTION

- 1.1 Scope
- 1.2 Project Background and Objectives
  - 1.2.1 The Mission
  - 1.2.2 Project Objectives
- 1.3 Project Results
  - 1.3.1 Data Availability
  - 1.3.2 Published Papers

### SECTION 2 - DATA PROCESSING

- 2.1 Data Collection
- 2.2 Processing Equipment
- 2.3 UTD Computer Program

### SECTION 3 - DATA SUMMARY

- 3.1 General
- 3.2 Mass 7 and 8 AMU
- 3.3 Distribution of H<sup>+</sup> and O<sup>+</sup>
- 3.4 Altitude Profile
- 3.5 Comparison with Other Experiments
  - 3.5.1 Comparison Passes
  - 3.5.2 Discussion of Comparisons
- 3.6 Neutral Hydrogen Distribution
- 3.7 Polar Wind

### SECTION 4 - INSTRUMENT DESCRIPTION

- 4.1 General
- 4.2 Operation
- 4.3 Calibration

## SECTION 1

### INTRODUCTION

#### 1.1 SCOPE

This report documents the work accomplished in reducing ionosphere composition data from the ion mass spectrometer experiment on Explorer XXXI satellite which was part of the ISIS program. The work was performed by The University of Texas at Dallas on contracts NAS 5-9444 and NSR 44-004-089 for the Office of Space Science and Applications, National Aeronautics and Space Administration.

Section 1, of this report, describes the project background and objectives, and the project results. Techniques used in processing the data are set forth in Section 2. Section 3 summarizes the experiment data, and a brief description of the ion mass spectrometer instrument is included as Section 4.

#### 1.2 PROJECT BACKGROUND AND OBJECTIVES

Magnetic deflection mass spectrometers have been used since 1964 to study the composition of the ionosphere from rockets and satellites. Such instruments have been successfully flown on four high altitude rockets and one satellite, the Explorer XXXI, which operated for 2-1/3 years in orbit.

##### 1.2.1 THE MISSION

On 29 November 1965 the Explorer XXXI satellite (Direct Measurements Explorer) was launched piggyback with the Canadian Alouette II Topside Sounder from the Western Test Range. The satellites were placed in an 80° prograde, 3000 km apogee, 500 km perigee orbit. The Explorer XXXI satellite contained experiments designed to measure directly certain properties of the earth's ionosphere. Various positive ion species in the ionosphere and their relative abundances were identified by the ion mass spectrometer.

The instrumentation flown in this experiment consists of a small magnetic sector-field mass spectrometer. There is no ion source employed in the instrument, since it is designed to measure the relative abundances of the positive ions formed in the upper atmosphere by natural processes.

Operating potentials are adjusted to permit thermal energy ambient ions to enter the mass spectrometer through an aperture in the side of the satellite. These ions then pass through the magnetic analyzer having an 1-1/2 inch (3.8 cm) radius (the permanent magnet has a field strength of 2200 gauss) and into an electron multiplier. A 5-decade logarithmic solid-state electrometer amplifier measures the output current from the electron multiplier. The mass spectrum from 1 to 20 amu (atomic mass units) is continually swept by an exponentially decreasing voltage having a 3-second period.

Data show that the ionosphere above 1000 kilometers usually consists of hydrogen ions as the predominant species. Between this altitude and perigee (500 kilometers) the dominant ion species shifts to atomic oxygen, with a significant amount of atomic nitrogen ions also present. Helium ions are present in small quantities at all altitudes. Other minor ions observed are those of 2, 7, 8, 15, 18, and 20 atomic mass units.

#### 1.2.2 PROJECT OBJECTIVES

Reducing raw satellite data from the ion mass spectrometer to a usable format that could be readily referenced was the objective of the project funded by NASA contract NSR 4-004-089. This work encompassed the following requirements.

- a. Writing a computer program for an IBM 360/50 computer which would operate on Experiment Input Tapes supplied by Goddard Space Flight Center.
- b. Recording the data in usable format on magnetic tapes.
- c. Plotting mission data on graphs for ready reference.
- d. Microfilming the data plots.
- e. Preparing a catalog of the microfilm reels.
- f. Delivering the finished microfilm to the National Space Science Data Center.

#### 1.3 PROJECT RESULTS

The ion mass spectrometer on Explorer XXXI has revealed in great detail the properties of the topside of the ionosphere in the

mass range of 1 to 20 amu. In addition to providing data on the composition of the ionosphere, the mass spectrometer made a contribution of considerable significance in indicating the existence of a "polar wind" of charged particles escaping from Earth, a phenomenon similar to that of the escape of "solar wind" particles from the sun.

Reduction of experiment data to a useful format makes new knowledge available to the world-wide scientific community. In addition to the wealth of reduced data, 10 papers have been published or presented to international scientific groups, and a paper on the polar wind is being prepared from the data.

### 1.3.1 DATA AVAILABILITY

Data from the ion mass spectrometer of the Explorer XXXI satellite has been deposited in the National Space Science Data Center (NSSDC) in the form of the SC4020 microfilm plots. These films are on 48 standard microfilm reels and are labeled according to date and time when the data were recorded. Cross references between recording times and refined world maps of the satellite orbit are available.

The NSSDC is located at Goddard Space Flight Center, Greenbelt, Maryland.

### 1.3.2 PUBLISHED PAPERS

The following listed papers have been published, based on data recovered as a result of contract NSR 44-004-089:

Hoffman, John H., "Composition measurements of the topside ionosphere," Science, 155, 322-324, 1967.

Hoffman, John H., "Ion composition measurements in the polar region from the Explorer XXXI satellite," Trans. Am. Geophys. Union, 49, 253, 1968.

Hoffman, John H., "Ion mass spectrometer on the Explorer XXXI satellite," Proceedings of IEEE, 57, June, 1969.

Donley, J. L., L. H. Brace, J. H. Hoffman, G. L. Wrenn, "Comparison of results of Explorer XXXI direct measurement probes," Proceedings of IEEE, 57, June, 1969.

Hoffman, J. H., C. Y. Johnson, J. C. Holmes, J. M. Young, "Daytime mid-latitude ion composition measurements," Trans. Am. Geophys. Union, 50, 259, 1969; J. Geophys. Res. 74, 6281, 1969 (Presented at 12th Plenary Meeting of COSPAR, Prague, May 1969).

Hoffman, J. H., "Measurements of the Mass 8 ion in the topside ionosphere," Trans. Am Geophys. Union, 50, 259, 1969.

Hoffman, J. H., "Mass Spectrometer measurements of ionospheric composition," Proceedings of the International Conference of Mass Spectroscopy, Kyoto, Japan, September, 1969.

Hoffman, J. H., "Studies of the composition of the ionosphere with a magnetic deflection mass spectrometer," Presented at Space Technology and Heat Transfer Conference, ASME, 70-Av/SpT-4, Los Angeles, June, 1970.

Hoffman, J. H., "Polar wind measurements," Presented at 52nd Annual AGU Meeting, Washington, D. C., April, 1971.

Hoffman, J. H., "Exospheric composition," McGraw-Hill Yearbook of Science and Technology, 111, 1968.

SECTION 2  
DATA PROCESSING

2.1 DATA COLLECTION

Data from the ion mass spectrometer was collected for over two years. Raw telemetry data was processed by Goddard Space Flight Center into 250 Experiment Input Tapes that were furnished to The University of Texas at Dallas. Figure 2-1 illustrates the data processing sequence.

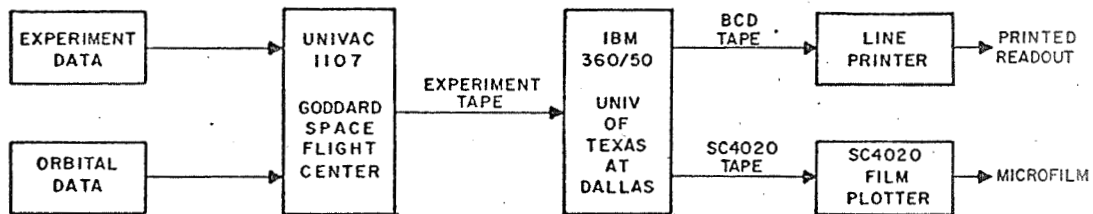


Figure 2-1. Data Processing Sequence

Telemetry data was taken from STRIPS decommutated tapes. Initial processing of telemetry data was done at the Goddard Space Flight Center using a special program for the UNIVAC 1107 which was written for the ion mass spectrometer experiment. A summary of this program is as follows, and figure 2-2 illustrates the primary logic flow:

Program execution begins with the main routine which sends control cards to determine the number of reels and files to be processed. Sense switches are checked to determine whether optional forms of output are desired.

The header record of the first file to be processed is read, and pass identification is extracted. The data records are searched for the first calibration cycle, and calibration coefficient are calculated. The tape is then backspaced to the start of the file.



A data record is read into the core and the records are unpacked by a Sleuth II routine and stored. The data is searched for a recharge to define a sweep start. If a sweep is not found, the next record is searched.

When a sweep period is defined, the data points are loaded into a two-dimensional array, the second column of which is the data to be searched, the first column is a data point count in the sweep.

The sweep of data is examined for peaks, valid peaks are scaled to ion currents, the spacecraft attitude is interpolated for the time of the peak.

When a sweep search has been completed, a mass position determination subroutine is called to determine the position of the ion masses using key peaks.

The peaks are then sorted into ion masses, adjusted by an instrument multiplication factor and converted to densities.

The peaks occurring in the sweep period are then output to the drum and on-line printer (if selected).

The next sweep is then unpacked into the two dimensional array and searched. This process continues to the end of the file.

Simultaneously with the spectrometer sweep data processing, the total ion collection plate data of a subcommutated word is unpacked, calibrated and scaled to ion density.

Housekeeping is performed to compensate for sweeps extending into the next record, calibration cycles during sweeps, etc. As calibrations occur, they are detected and new coefficients determined.

The ion densities of ten masses are plotted on the SC4020 plotter, each plot containing two minutes of data.

Successive files and tapes are processed according to the parameters input on cards.

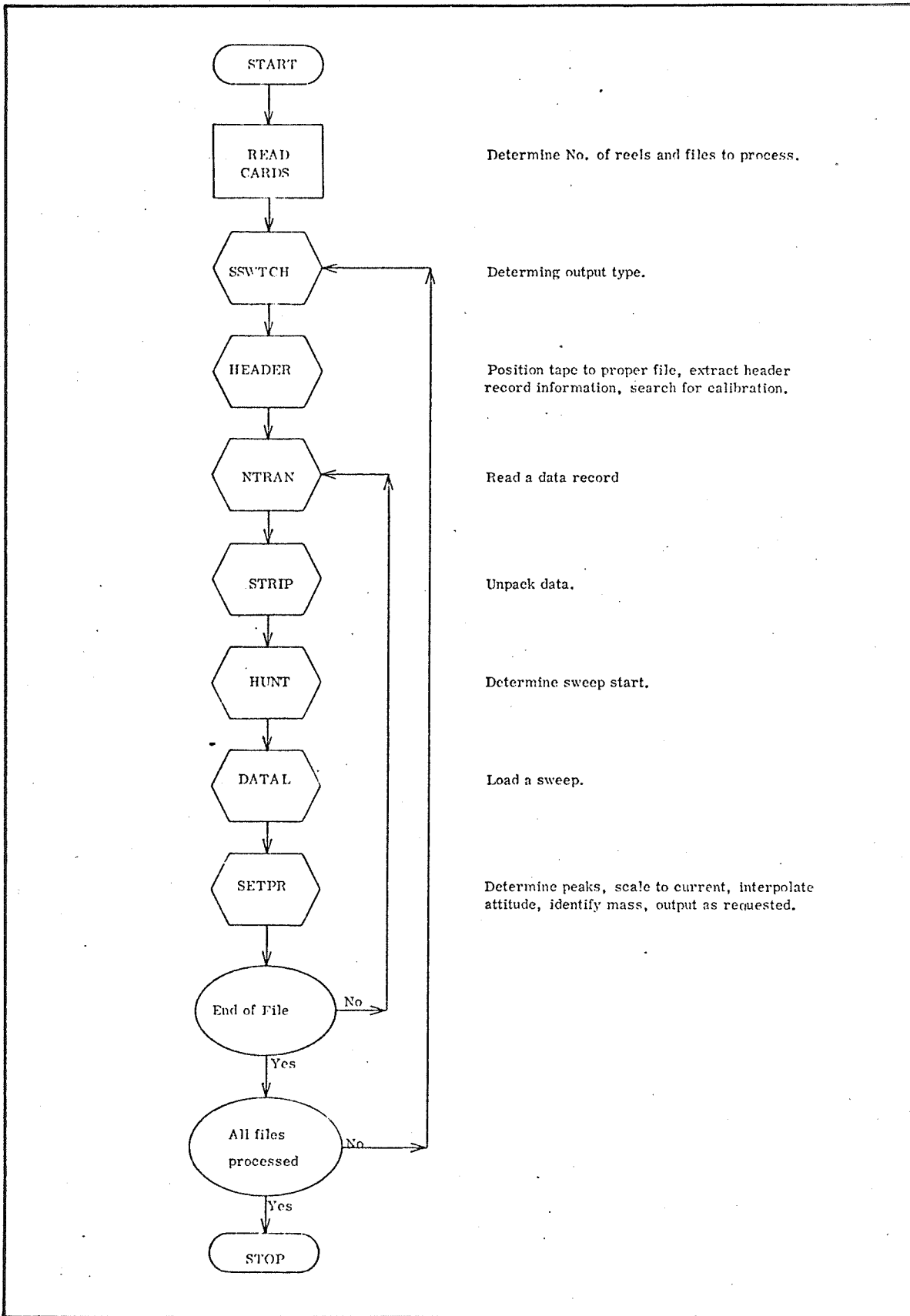


Figure 2-2. Experiment Input Tape Flow Diagram

## 2.2 PROCESSING EQUIPMENT

Primary processing equipment used on NASA Contract NSR 44-004-089 was an IBM 360/50 and a Stromberg-Carlson SC4020 Film Plotter. It will be noted that the SC4020 Film Plotter has been acquired by Datagraphics, Inc. and redesignated as their model SD4020. The Stromberg-Carlson designation has been used throughout this report to be consistent with earlier documentation.

## 2.3 UTD COMPUTER PROGRAM

After a small number of tapes were processed at GSFC, the data reduction operation was moved to UTD. A program for the UTD IBM 360/50 was written to reduce the data on the Experiment Input Tapes supplied by GSFC. Figures 2-3 and 2-4 illustrate the primary areas of the procedure.

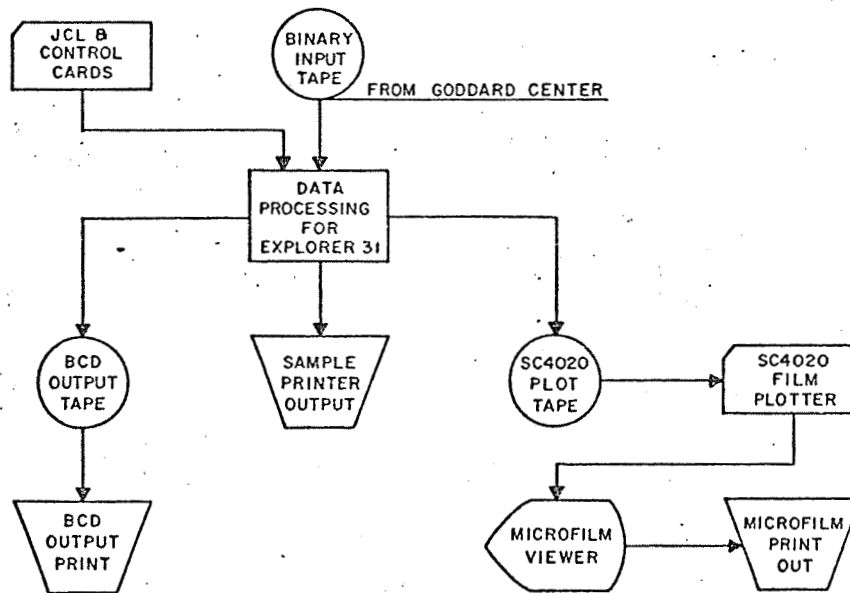


Figure 2-3. Explorer XXXI Data Processing Procedure

The program first searches the input tape for amplifier calibration data which is used to compute the coefficients of a conversion equation which calculates ion currents from the peak amplitude. Next, the program finds the position and amplitude of each peak in the spectrum, identifies each peak by mass number and by applying appropriate correction factors calculates the absolute concentration of each ion species observed.

Output of the program is in three formats. First, a single page monitor of the data from each file on the tape (one file is equivalent to one satellite pass over a receiving station) is printed out listing sweep number, ion peak amplitude, ion concentration, mass number identification and angle of attack as a function of time. Also, orbital data are listed every eight seconds. This page serves as a check or quality control on the data processing operation.

The second output is a BCD data tape containing the same information as the single page monitor. The format is also identical but this tape contains all of the data from a given pass. The data are stored on the BCD tapes as a convenient interim storage format from which analyses may be performed. In this form the data may be conveniently sorted and plotted as a function of any of the parameters listed on the tape, such as time, altitude, latitude, local time, etc. Listing of the data on the BCD tape is a simple, fast, direct I-O operation on the computer.

The third output from the data processing program is an Stromberg-Carlson SC4020 plot tape, which, when plotted on the SC4020 plotter, produces microfilm plots of the concentration of each ion species as a function of time. Each graph contains 120 sec of data and a normal complete pass will produce five graphs. These microfilm graphs are the most useful format in which the data could be stored, for they clearly show the roll modulation effect and contain absolute concentrations of each ion species.

- I. Get three tapes.
  - A. Input (BINARY from Goddard Center)
  - B. BCDØUT PUT (Scratch new tape)
  - C. PLØT ØUTPUT

| UNIT                    | 181                 | 182                      |
|-------------------------|---------------------|--------------------------|
| BCDØUTPUT<br>(FT15F001) | INPUT<br>(FT09F001) | PLØTØUTPUT<br>(FT10F001) |

II. Setting up job for the run.

JCL

- In "FT09F001" change "VØLUME=SER=XXXXXX", which is the current input tape number.
- In "FT15F001" change "LABEL" parameter where file number should be put in sequence.

Example:

```
//G.FT15F001 DD .....,.....,LABEL=(05,BLP),.....
//G.FT15F002 DD .....,.....,LABEL=(06,BLP),.....
                etc.
```

- In "FT10F001" change "VØLUME=SER=XXXXXX", which is the current plot tape number.

Control-Cards

```
//G.FT01F001 DD *
```

Card Sequence

- 1 \* 2(E10.3) FØRMAT  
It contains the 1st and last scaling labels of plot.
- 2 \* through 11  
There are 10 cards containing AINTER and ASLOPE for 10 different masses.  
FØRMAT (F5.2,E10.2)
- 12 It contains IYK \*\*, IPØSC \*, LIMH \* with 3(15) FØRMAT
- 13 through 22.  
These are the ID Information  
13: EXPLØRER 31  
    ↑  
    29  
    Col.  
    15. 3 \*\*  
    ↑   ↑  
    69 72  
    Col. Col.

This is a run number.

14: BLANK CARD

Figure 2-4. Data Processing Sequence

15: INVESTIGATED

↑  
35  
Col.

16: BY

↑  
40  
Col.

17: JH HOFFMAN

↑  
36  
Col.

18: PROGRAMMED

↑  
36  
Col.

19: AND EDITED PROGRAMS

↑  
31  
Col.

20: BY

↑  
40  
Col.

21: YOUNG RHEE

↑  
36  
Col.

22: BLANK CARD

23\*\* Card on Down.  
Control cards which indicate which files are to be processed.  
(FORMAT (3(I5)))

Example:

|      |      |      |                              |
|------|------|------|------------------------------|
| 1    | 15   | 0    |                              |
| 1    | 23   | 0    |                              |
| 0    | 0    | 0    | ----- This is the last card. |
| ↑    | ↑    | ↑    |                              |
| 5    | 10   | 15   |                              |
| Col. | Col. | Col. |                              |

The quantities in Column 5 and Column 15 are not to be changed.  
The quantity in Column 9 and 10 indicate the files to be processed.

/\*

Note: \* This information can be changed by Dr. Hoffman's instructions only.

\*\* This information can be changed whenever it is necessary according to tape informations to be processed.

Figure 2-4. Data Processing Sequence

## SECTION 3

### DATA SUMMARY

#### 3.1 GENERAL

It has been found from the Explorer XXXI data that below 1000 km  $O^+$  is the dominant ion species in the ionosphere (Fig. 3-1).  $N^+$  varies from 5 to 30 percent of the  $O^+$  and  $H^+$  is generally a minor constituent, occasionally as low as 5 percent of the  $O^+$ .

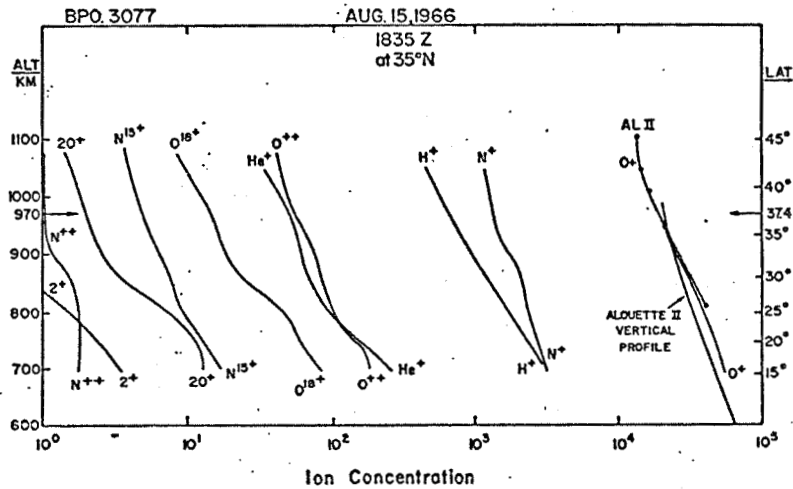


FIGURE 3-1. Typical low-altitude data showing ion concentration versus altitude and latitude. Ten different ion species are observed. Alouette II electron concentrations are also given.

Above about 2000 km at mid to low latitudes, the ionosphere generally consists of the order of 99 percent  $H^+$ , the remainder being  $He^+$ ,  $D^+$ , and  $8^+$ . The crossover altitude between  $O^+$  and  $H^+$  is quite variable, being a function of several parameters.  $He^+$  is a very minor constituent at all altitudes being of the order of a few percent to less than 1 percent.

Ten different ion species have been observed between 1 to 20 amu at 1( $H^+$ ), 2( $D^+$ ), 4( $He^+$ ), 7( $N^{++}$ ), 8( $O^{++}$  or  $He_2^+$ ), 14( $N^+$ ), 15( $N_{15}^+$ ), 16( $O^+$ ), 18( $H_2O^+$  or  $O_{18}^+$ ), and 20( $Ne^+$ ) amu (1)<sup>1</sup>. All except mass 15 are shown in Figure 3-1. The sensitivity of the Explorer XXXI mass spectrometer to  $H^+$  ions is of the order of 0.3/cc and to  $O^+$  ions of the order of 10/cc.

<sup>1</sup>Underlined numbers in parentheses designate references at the end of Section 3.

### 3.2 MASS 7 and 8 AMU

An ion peak at mass 8 amu is frequently observed in the data, always at low altitudes and not infrequently above 2000 km. In regions where  $O^+$  is the dominant constituent, the mass 8 ion is identified as  $O^{++}$ , formed by photoionization of  $O^+$ . Its relative abundance is of the order of a few  $\times 10^{-3}$  of the  $O^+$ . Likewise, a peak at mass 7 is identified as  $N^{++}$ . These are the first data in which the doubly charged constituents have been observed. From 2200 to 3000 km, the mass 8 ion distribution, at a concentration of the order of 1/cc, favors the southern hemisphere in January and February, whereas in July and August, it is more equally distributed.  $O^+$  is found above 2200 km only in the summer northern hemisphere and, then, almost always above 50 deg N geomagnetic latitude. On the other hand,  $He^+$  appears at all times in both hemispheres.

### 3.3 DISTRIBUTION OF $H^+$ and $O^+$

At altitudes from 2200 to 3000 km, the concentration of  $H^+$  and  $O^+$ , as a function of geomagnetic latitude and season, are shown in Figures 3-2 and 3-3, respectively. In the local summer, the concentration of  $H^+$  decreases abruptly at about 60 deg. and the concentration of  $O^+$  rises correspondingly making  $O^+$  the dominant ion species.  $O^+$  is seldom observed at these altitudes except in the regions around 60 deg and northward. These regions of  $O^+$  dominance are not particularly structured in the summer, but the total ion concentration is almost two orders of magnitude below that at lower latitudes where  $H^+$  is the dominant species.

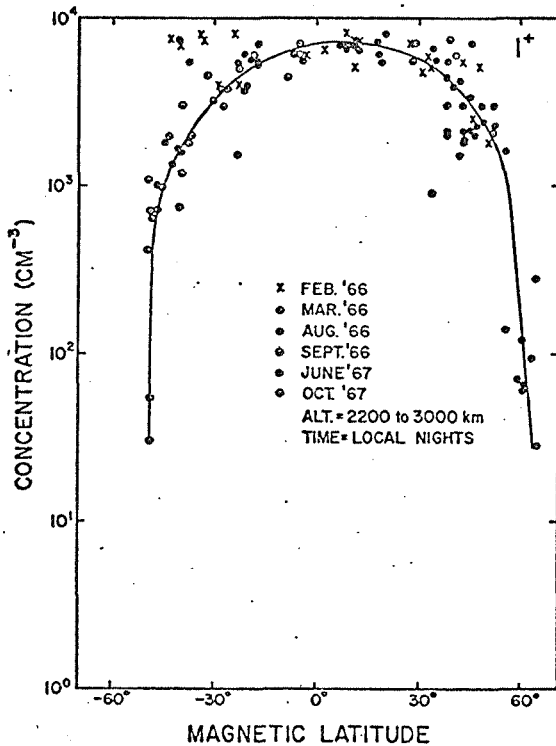


Figure 3-2. Distribution of  $H^+$  ions above 2200 km as a function of geomagnetic latitude and season

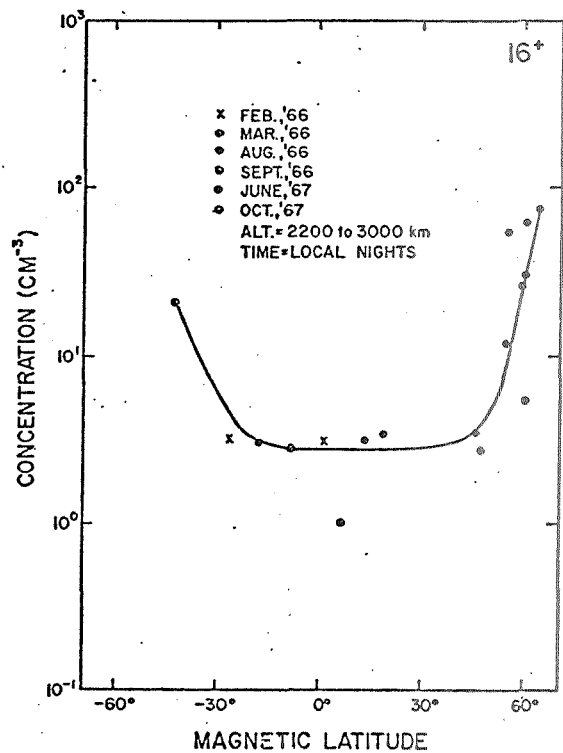


Figure 3-3. Distribution of  $O^+$  ions above 2200 km as a function of geomagnetic latitude and season



In the winter polar region above 2500 km,  $O^+$  has also been observed to become the dominant ion constituent in a highly structured narrow region between 75 and 85 deg N geomagnetic latitude. Figure 3-4 shows such a situation. The  $H^+$  concentration exhibits 1 to 2 orders of magnitude trough at 70 deg N geomagnetic latitude, whereas the  $O^+$  region lies to the north, but not to the south, of the trough. There is evidence from the phase difference of the maxima in the roll modulation curves (Figure 3-5) in this structured region and in the summertime regions of  $O^+$  dominance, that  $H^+$  ions are flowing upward with a velocity of 10 to 15 km/sec. This is the first experimental evidence for the polar wind (2).

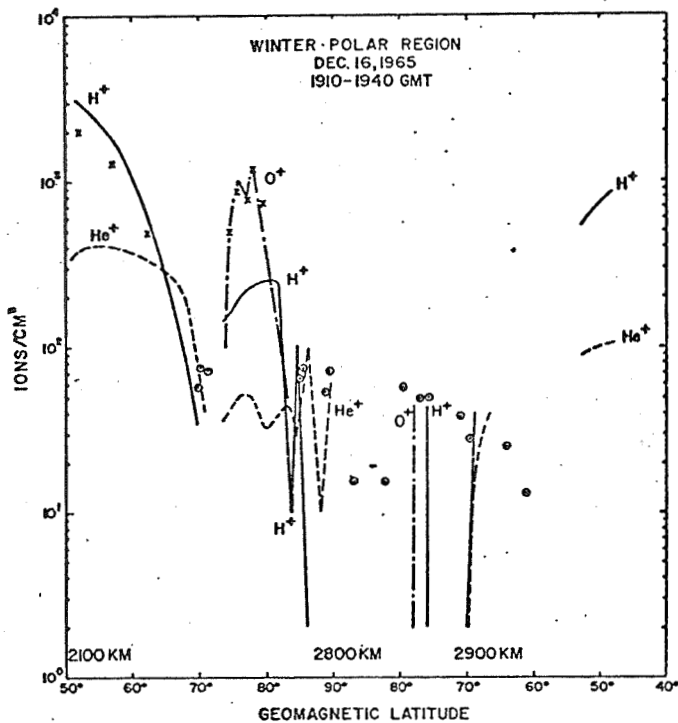


Figure 3-4. Ion concentrations versus geomagnetic latitude for northern polar region. X's are Alouette II data reduced by standard method. O's are Alouette II data by Hagg method. In region around 80 to 85 deg N,  $H^+$  ions have an upward drift velocity of 10 to 15 km/sec.  $N^+$  is also observed at concentration of 6 percent of  $O^+$ , (not shown in figure)

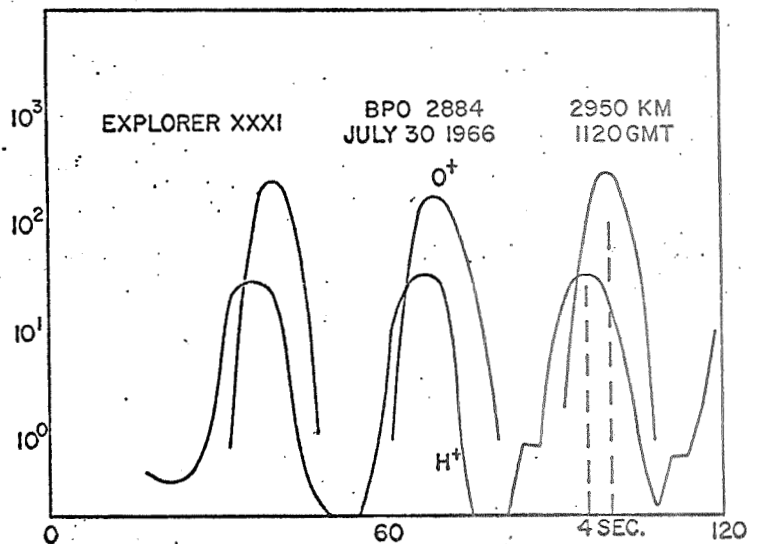


Figure 3-5. Ion concentration versus time showing phase difference in the roll modulation maxima of  $H^+$  and  $O^+$

### 3.4 ALTITUDE PROFILE

An Argo (Javelin) rocket was launched from Wallops Island, Virginia at 1828 GMT, August 15, 1966, to rendezvous with a pass of the Explorer XXXI and Alouette II satellites. Identical magnetic mass spectrometers on the rocket and Explorer XXXI satellite measured the composition of the ionosphere, while the Alouette II topside sounder provided electron density profiles.

Data were obtained on the rocket flight from 425 km on the up-leg to the peak of flight, 723 km, and down to 130 km on the descent. Figure 3-6 shows a plot of the concentrations of each ion species as a function of rocket altitude with the direction of the arrows indicating up-or-down-leg of the flight. The solid curve to the right in the figure shows the electron density measured by the Alouette II Topside Sounder (3) matched to the Wallops Island Ionosonde (4) data taken at the time of flight of the rocket.

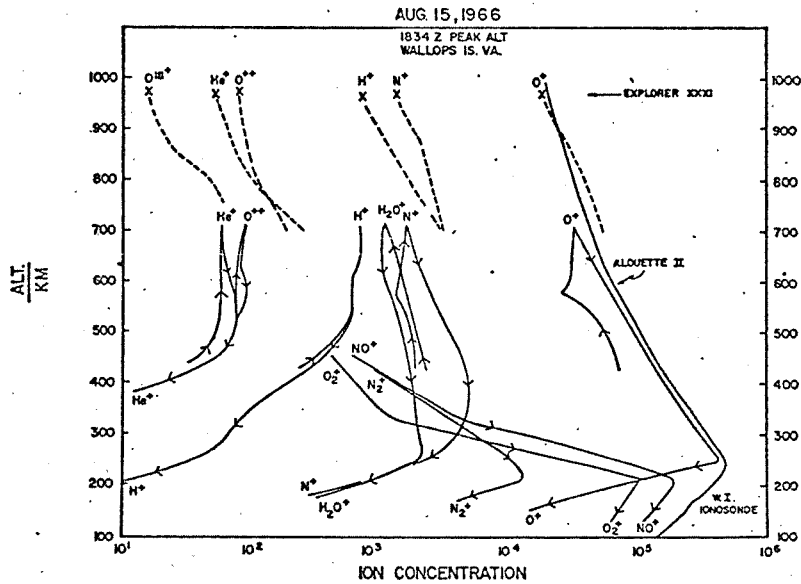


Figure 3-6. Ion concentration as a function of altitude showing both the rocket data (solid lines) and the satellite data (broken lines). X's refer to the satellite data at the point of intersection of the two trajectories. The Alouette II electron density from the topside sounder experiment is matched to the Wallops Island ionosonde data at the F2 maximum

The Explorer XXXI ion composition results, plotted as a function of height, are shown at the top of Figure 3-6 as dashed lines. The X's are the values at the intersection of the rocket and satellite trajectories.

The  $O^+$  profile follows the Alouette II  $N(h)$  profile reasonably well.  $O^+$  is by far the dominant constituent, being 94.2 percent (including 2.8 percent  $H_2O^+$ ) of the total ion concentration at 700 km.  $N^+$  is next at 4.1 percent, and  $H^+$ , being a very minor constituent, even at the satellite altitude, indicates that its crossover with  $O^+$  lies well above 1000 km. A mass 8 ion is observed throughout the rocket data and is identified as  $O^{++}$ . Its scale height is very large (actually it is negative but could be infinite within the experimental error) indicating a doubly charged constituent of half the mean ion mass. It is unlikely that the mass 8 is  $He_2^+$ , since its concentration is greater than that of  $He^+$ . The very low  $He^+$  concentration shown here, 0.15 percent, is typical of the  $He^+$  values observed by the Explorer XXXI satellite in mid-latitude regions.

The molecular ion constituents,  $NO^+$ ,  $O_2^+$ , and  $N_2^+$  all have maximum concentration below the  $F_2$  maximum. There is a significant change of slope in the  $NO^+$  and  $O_2^+$  at about 350 km, but not in the  $N_2^+$  data. The data points below 200 km are subject to greater uncertainties than those at higher altitudes due to the increased rocket velocity and correspondingly greater roll modulation of the ion peak amplitudes. The rocket is also tumbling and, therefore, yields relatively few points when the angle of attack is sufficiently small to enable a roll modulation correction to be made. The result is that the altitude of the maxima of the molecular constituents may be in error by up to 30 km.

### 3.5 COMPARISON OF RESULTS WITH OTHER EXPERIMENTS

An important objective of this mission was the simultaneous measurement of ionospheric parameters by direct measurement probes and electron density profiles measured by the topside sounder experiment on Alouette II and reported by Donley, et al (5). The close proximity of the two satellites provided an excellent opportunity for such simultaneous data coverage for several months after launch. The orbital separation was about 105 seconds (about 800 km) two months after launch.

Explorer XXXI was instrumented with direct measurement probes which provided measurements of the major ionospheric parameters through different techniques. The experiment complement, measured parameters pertinent to the comparison, nominal data accuracies, and principal investigators are as follows:

- a. Planar ion trap - ion density ( $\pm 10$  percent), temperature ( $\pm 150^\circ\text{K}$ ), and composition; J. L. Donley.
- b. Planar electron trap - electron density ( $\pm 20$  percent) and temperature ( $\pm 200^\circ\text{K}$ ); J. L. Donley.
- c. Cylindrical electrostatic probes - electron density ( $\pm 10$  percent) and temperature ( $\pm 150^\circ\text{K}$ ); L. H. Brace and J. A. Findlay.
- d. Magnetic ion mass spectrometer - ion density ( $\pm 10$  percent) and composition; J. H. Hoffman.
- e. Planar Langmuir plate - electron temperature ( $\pm 100^\circ\text{K}$ ); A. P. Willmore and G. L. Wrenn.
- f. Spherical ion probe - ion density ( $\pm 2$  percent), temperature ( $\pm 200^\circ\text{K}$ ), and composition; A. P. Willmore and G. L. Wrenn.

### 3.5.1 COMPARISON PASSES

For the purpose of data intercomparison and passes listed in Table 3-1 were selected for detailed study. These passes were selected on the basis that all experiments were operating satisfactorily and good aspect data and simultaneous Alouette II sounder data were available. For the passes selected the maximum in-orbit separation time of the satellite was less than 105 seconds, and regions of rapidly varying ionospheric conditions have been avoided. A wide variety of geographic locations and plasma density conditions are covered. The spacecraft was in sunlight for all passes. The northern auroral regions, which represent a large percent of data coverage, have been excluded from this initial comparison study since such passes were at apogee altitudes and consequently very low plasma densities (about  $10^2/\text{cc}$ ) which are below the sensitivity threshold of some experiments were encountered.

Table 3-1. Details of Comparison Passes

| Station                | Pass | Date    | Universal Time |      | Height (km) |      | Latitude (Degrees) |       | Longitude (Degrees) |       |
|------------------------|------|---------|----------------|------|-------------|------|--------------------|-------|---------------------|-------|
|                        |      |         | Start          | End  | Start       | End  | Start              | End   | Start               | End   |
| Kano (KNO)             | 368  | 30DEC65 | 0449           | 0458 | 1555        | 2120 | 2.2                | 27.7  | 12.3                | 15.0  |
| Orroral (RAL)          | 546  | 14JAN66 | 0631           | 0638 | 709         | 538  | -26.1              | -53.1 | 144.6               | 151.6 |
| Winkfield (WNK)        | 550  | 14JAN66 | 1411           | 1418 | 2224        | 1797 | 55.5               | 36.9  | 9.0                 | 14.6  |
| Blossom Point<br>(BPO) | 730  | 29JAN66 | 1842           | 1849 | 1359        | 935  | 44.6               | 21.1  | -80.8               | -76.4 |
| Santiago (SNT)         | 730  | 29JAN66 | 1900           | 1905 | 537         | 525  | -20.9              | -46.9 | -71.3               | -67.6 |

### 3.5.2 DISCUSSION OF COMPARISONS

The comparison results presented in Table 3-2 although few in number are not sufficient for a statistical study, are felt to be typical of the results from the Explorer XXXI. In the measurement of plasma density, electron temperature and ion composition, there is no significant systematic disagreement between the various probes that cannot be recognized as arising from sensitivity or limiting considerations. There are, however, some random disagreements which require additional investigation. In general plasma density results were within  $\pm 20$  percent of simultaneous Alouette II density measurements with occasional variations of up to about  $\pm 50$  percent. Electron temperature results generally agreed to within  $\pm 10$  percent with maximum variations of up to  $\pm 20$  percent.

Of the probes employed, four used planar flush-mounted sensors (ion trap, electron trap, magnetic mass spectrometer, and Langmuir plate). The cylindrical electrostatic probes and the spherical ion probe were mounted on short booms about one foot from the satellite surface. This indicates that correct plasma diagnostics can be achieved for flush sensors operating within the satellite sheath. It is to be noted, however, that electron density values from the planar Langmuir plate (these results are not included in this paper) are always a factor of from 2 to 5 lower than the correct value. The planar electron trap appears to give reasonable results. The only significant difference in the two planar sensors is that the electron trap employs a swept surface area of about  $55 \text{ cm}^2$  while the Langmuir plate swept surface area is about  $12 \text{ cm}^2$ . This suggests that satellite sheath penetration was not adequately achieved with the smaller area.

Table 3-2. Ion Composition Results

| Station       | Pass | Time | Magnetic Spectrometer |                 |                |                | Ion Trap       |                | Spherical Probe |                |
|---------------|------|------|-----------------------|-----------------|----------------|----------------|----------------|----------------|-----------------|----------------|
|               |      |      | H <sup>+</sup>        | He <sup>+</sup> | N <sup>+</sup> | O <sup>+</sup> | H <sup>+</sup> | O <sup>+</sup> | H <sup>+</sup>  | O <sup>+</sup> |
| Kano          | 368  | 0450 | 99                    | 1               | —              | —              | 100            | —              | 100             | —              |
|               |      | 0456 | 99                    | 1               | —              | —              | 100            | —              | 100             | —              |
| Orroral       | 546  | 0632 | 5                     | —               | 6              | 89             | 5              | 95             | 6               | 94             |
|               |      | 0636 | 1                     | —               | 6              | 93             | —              | 100            | 1               | 99             |
| Winkfield     | 550  | 1412 | 78                    | 12              | 2              | 8              | 84             | 16             | 100             | —              |
|               |      | 1417 | 86                    | 7               | 1              | 6              | 96             | 4              | 100             | —              |
| Blossom Point | 730  | 1841 | 6                     | 1               | 7              | 86             | 7              | 93             | 3               | 97             |
|               |      | 1844 | 23                    | 3               | 5              | 69             | 28             | 72             | 29              | 71             |
|               |      | 1848 | 35                    | 3               | 3              | 59             | 36             | 64             | 43              | 57             |
| Santiago      | 730  | 1902 | 1                     | —               | 2              | 97             | —              | 100            | 2               | 98             |
|               |      | 1904 | 1                     | —               | 3              | 96             | —              | 100            | 2               | 98             |

The general agreement in electron density measurements between the Alouette II sounder, cylindrical probe, and electron trap also indicates that large magnetic field orientation effects are not present. The anisotropy noted in electron temperature measurements could indicate a magnetic field influence.

The only area of major disagreement is in the measurement of ion temperature. The planar ion trap results are significantly greater than the results from the boom-mounted spherical probe. Although no serious conflict occurs in the relative trends observed, it is likely that in both cases there are measurement problems which preclude absolute significance for H<sup>+</sup> ion temperature results. A limited comparison of the measured ion temperatures with radar backscatter results has been attempted. This indicates that the spherical probe results for O<sup>+</sup> may be somewhat low. No comparison data are available to resolve discrepancies in the measured H<sup>+</sup> temperatures. A possible source of error in the ion trap measurement is sheath curvature. The analysis assumes a planar sheath. Knudsen (6) has considered such perturbations to ion temperature measurements with planar traps and found the resultant error quite small. Additional effort is required to assess completely the ion temperature comparisons.

### 3.6 NEUTRAL HYDROGEN DISTRIBUTION

In the lower region of the ionosphere, H<sup>+</sup> and O<sup>+</sup> are in chemical equilibrium through the well-known charge exchange reaction (8),

$$\frac{n(H^+)}{n(O^+)} = \frac{9}{8} \frac{n(H)}{n(O)} \quad (1)$$

Since equation (1) represents both the source and sink for H<sup>+</sup>, the scale height of the ratio of n(H<sup>+</sup>) to n(O<sup>+</sup>) is characterized by an effective mass of 15 amu and is a function of the neutral gas temperature. From the observed scale height of 53 km', the temperature of the neutral gas is 940 K. It is assumed that T<sub>g</sub> = T<sub>i</sub> here.

From the model of the neutral atomic oxygen distribution and with the aid of equation (1), the neutral hydrogen distribution can be calculated for the region of chemical equilibrium. The model atmosphere of Harris and Priester (1962) at a temperature of 962 deg and 10.7 cm flux of 100 x 10<sup>-22</sup> W/sq m cps was used for the atomic oxygen profile which is shown in Figure 3-7. The measured oxygen values of Krankowsky, Kasprzak, and Nier (7) for a summer daytime rocket flight

at White Sands are given as dots in the figure to which the Harris and Priester model  $n(O)$  was normalized at 200 km, the normalization constant being 0.77.

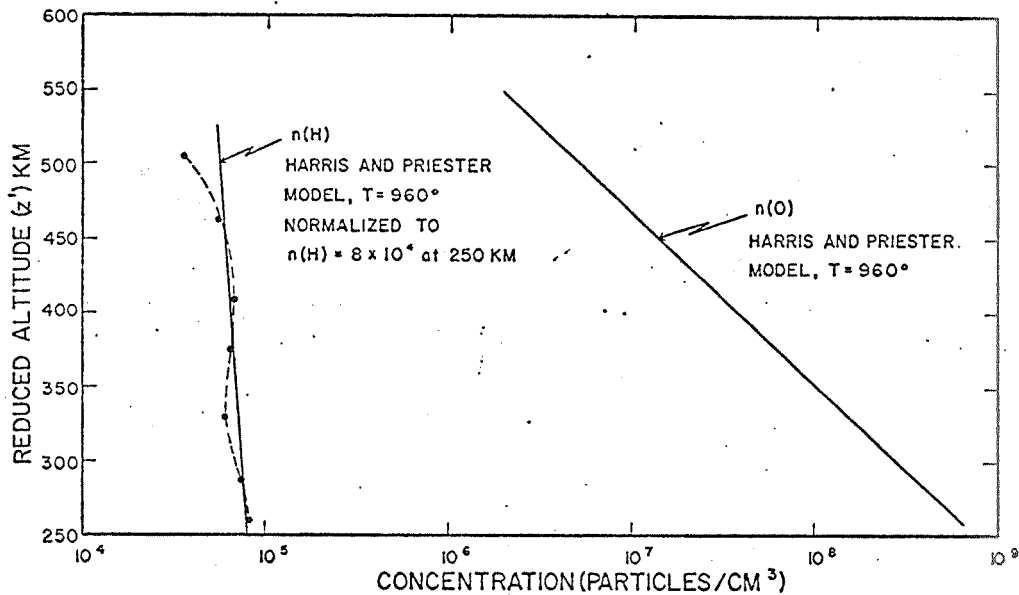


Figure 3-7. Concentrations of O and H as a function of reduced altitude. The model  $n(O)$  is normalized to a rocket measurement (see text) at 200 km. Calculated  $n(H)$  is the dashed curve. Model  $n(H)$  is normalized to calculated value at 250 km'. Normalization factor is 4.6.

The calculated atomic hydrogen distribution from equation (1) and the  $n(O)$  curve is then given as the dashed curve in Figure 3-7. For comparison, the Harris and Priester model hydrogen profile is given as the solid  $n(H)$  curve normalized to the calculated  $n(H)$  at 250 km'. The normalization factor here is 4.6. The calculated values agree well with the model up to 450 km' where the significant departure indicates that the  $H^+$  is no longer in chemical equilibrium with  $O^+$ .

Krankowsky, et al. quote a probably accuracy of 25 percent for the atomic oxygen number density; the  $n(H^+)/n(O^+)$  ratio probable accuracy is 20 percent. Therefore, the  $n(H)$  probable accuracy is 45 percent.

In comparing the present results with those of other mass spectrometer flights in a similar time period, it is seen that there is a difference in the  $n(H^+)$  measurements, the present result being lowest. The in-flight calibration tends to indicate that a mass spectrometer is overly sensitive to light mass ions compared to  $O^+$ .

### 3.7 POLAR WIND

Section 3.3 referred to the first experimental evidence for the existence of the polar wind being determined from the data from this experiment. The phase shift between the roll modulation maxima for  $H^+$  and  $O^+$  and the usual dominance of  $O^+$  are direct indications that the polar wind is flowing. Figure 3-8 shows the locations in the northern polar region where the phase shift occurs in the summer. In general, broad areas above  $62^\circ$  invariant latitude exhibit the phenomenon. Figures 3-9 and 3-10 show a crossover between  $H^+$  dominant and  $O^+$  becoming dominant as the invariant latitude increases. There is no phase shift in Figure 3-9, but a significant phase shift is evident above  $65^\circ$  in Figure 3-10. Also, the ion concentrations at the higher latitudes are below  $10^2/cm^3$  which is an order of magnitude below typical, mid-latitude values. A detailed look at the phase shifts between  $H^+$  and  $O^+$  is seen in Figure 3-11. It should be noted that the magnitude of the  $H^+$  roll modulation is very large, 2 orders of magnitude, as compared with values less than 5 as seen in the right-hand side of Figure 3-9. Figure 3-12 shows the phase shift onset on a magnetically quiet day being rather slow where as on a disturbed day (Figure 3-13) the onset is abrupt, being accompanied by a sudden decrease in  $H^+$  concentration and a corresponding rise in  $O^+$ .

Figure 3-14 is a histogram of the frequency of occurrence of the phase-shift,  $O^+$  dominance as a function of L. At L below 4 there is little evidence of a phase shift whereas above the value the phase shift is the usual condition, although a small number of cases are observed without phase shift although  $O^+$  is still the dominant ion species.

Wintertime distribution of polar wind areas of the northern polar region is given in Figure 3-15. The onset of the wind is at a somewhat higher latitude than in summer, and is concentrated in a fairly narrow band as is evidenced in Figure 3-16. The phase shifts are generally larger in winter indicating higher  $H^+$  velocities.

Figure 3-17 is a plot of the earth's magnetic field showing the region where the polar wind ions flow along open magnetic field lines. Electric fields established parallel to magnetic field lines tend to increase the scale height of  $O^+$  and accelerate  $H^+$  ions along the field lines giving rise to the phase shift phenomenon and to the  $O^+$  dominance at high altitudes (3000 km). Total ion concentration is decreased due to the lesser scale height of  $O^+$ , even though it is larger than at mid-latitudes, than  $H^+$ , and the flow of  $H^+$  out of the polar region.

Theoretical work on the polar wind has been done principally by Banks (9), and has generally been able to explain the results from the Explorer XXXI ion composition experiment.



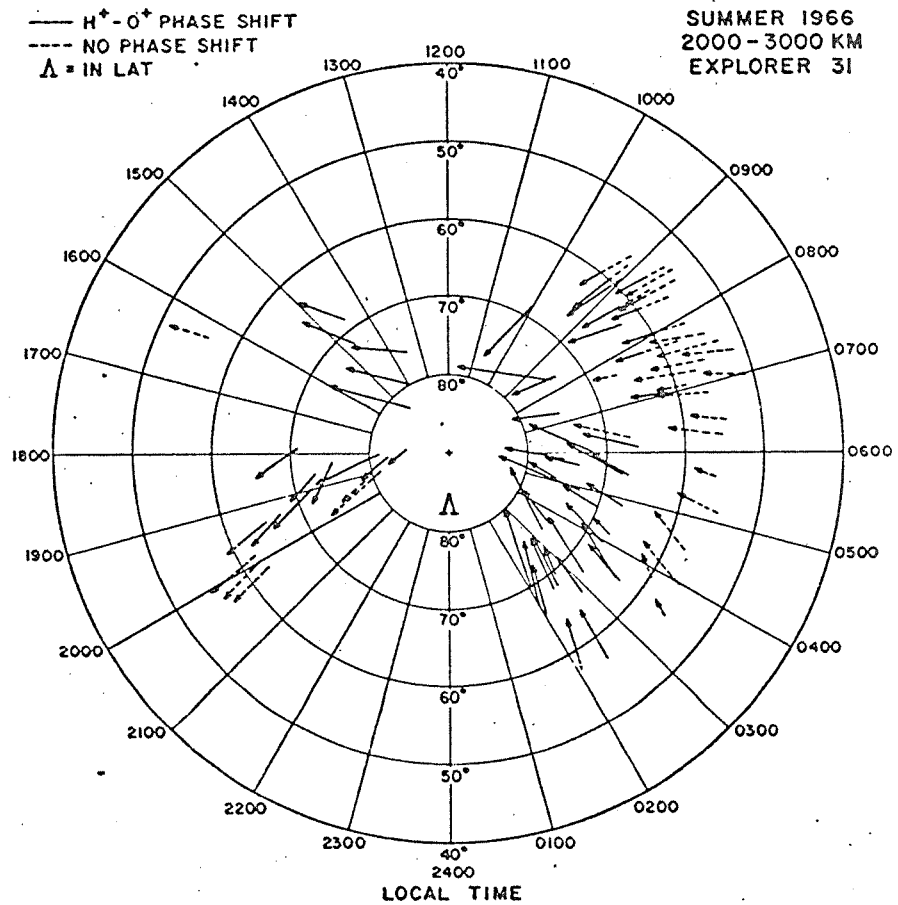


Figure 3-8. Observations of polar wind flow in the summer polar cap. All available data is shown with direction of satellite pass indicated by arrow. Solid line indicates presence of ion flow, while the dotted line indicates its absence.



JUN. 27, 1966

EXPLORER 31

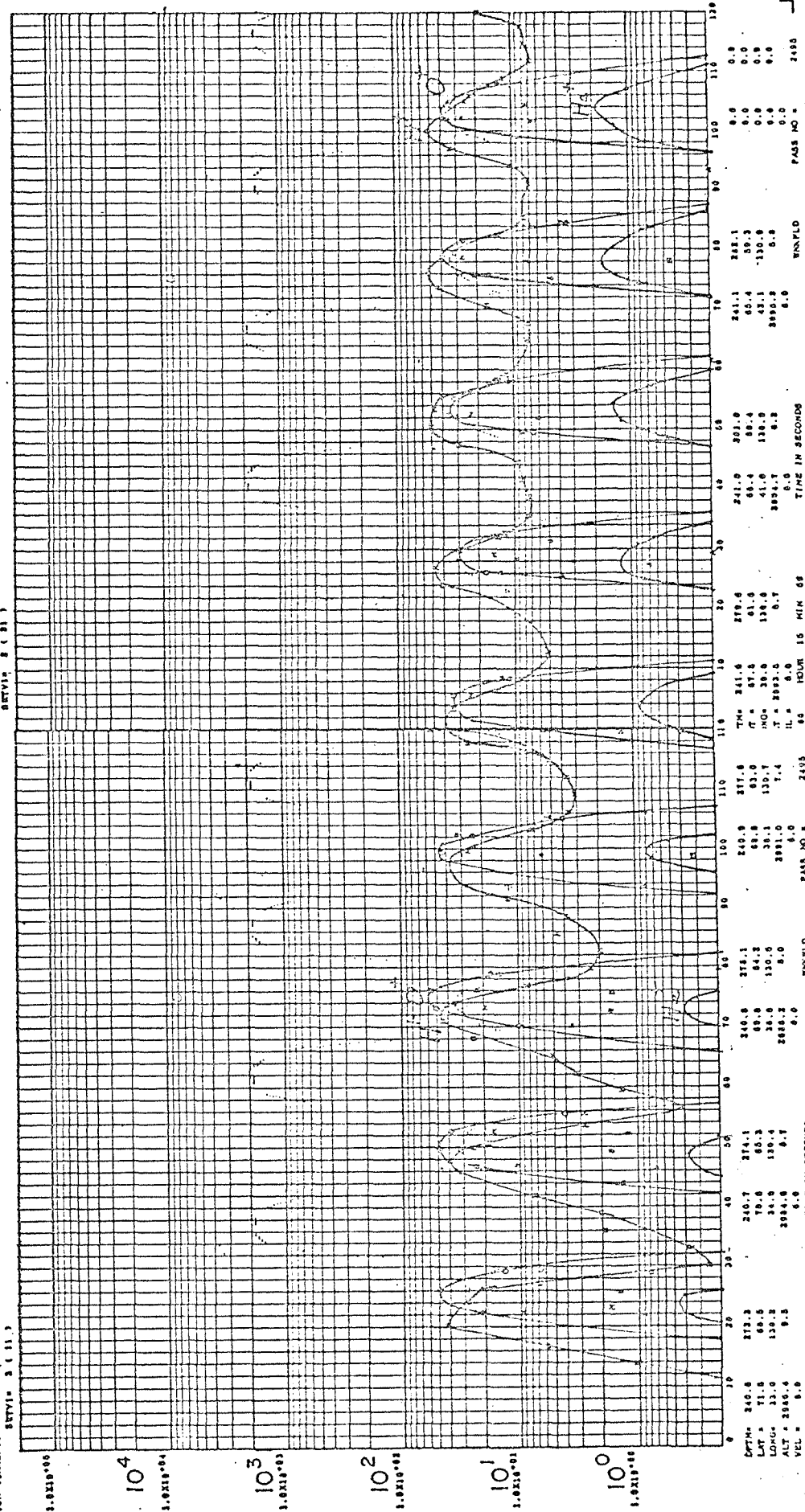
J. HOFFMAN, SCAS

17-3 010 473

J. HOFFMAN, SCAS

17-3 011 474

10X CURRENTS  
SERVIS = 3 ( 11.3 )



JUN 27, 66 HOUR 16 MIN 57

68°

IN LAT

71°

65°

Figure 3-10. H+ and O+ crossover with phase shift.

AUG. 8, 1966

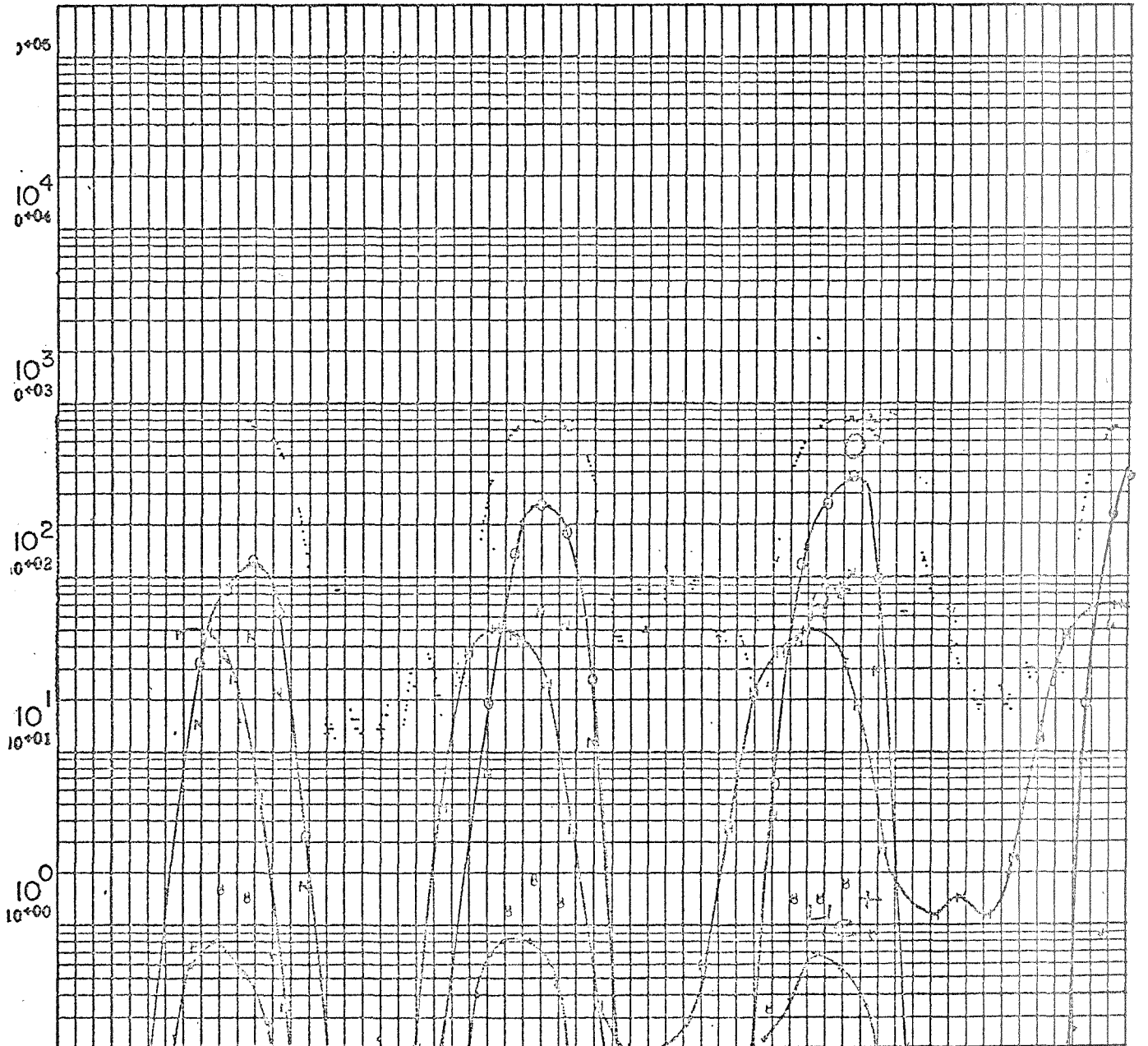
EXPLORER 31

REPORTS

J. HOFFMAN, SCAS

19-2 102

BETV1= 0 ( 11 )



|              |      |          |      |                 |      |        |      |           |      |        |      |        |
|--------------|------|----------|------|-----------------|------|--------|------|-----------|------|--------|------|--------|
| 0            | 10   | 20       | 30   | 40              | 50   | 60     | 70   | 80        | 90   | 100    | 110  | 120    |
| DPM= 152.2   | 74.2 | 155.6    | 75.4 | 159.6           | 76.9 | 164.0  | 78.4 | 168.4     | 79.9 | 172.8  | 81.4 | 82.9   |
| LAT = 65.4   | 75.0 | 65.6     | 75.9 | 67.6            | 76.7 | 68.7   | 77.6 | 69.6      | 78.5 | 70.5   | 79.4 | 80.3   |
| LONG= -45.2  | 42.5 | -44.0    | 45.8 | -42.7           | 49.6 | -41.2  | 54.0 | -39.6     | 58.4 | -38.0  | 62.8 | 67.2   |
| ALT = 2729.1 | 16.6 | 2710.0   | 18.2 | 2690.4          | 20.0 | 2670.1 | 21.9 | 2650.0    | 23.8 | 2630.0 | 25.7 | 2610.0 |
| VEL = 6.2    |      | 6.2      |      | 6.2             |      | 6.2    |      | 6.2       |      | 6.2    |      | 6.2    |
| 8 AUG. 66    | HR   | 7 MIN 58 |      | TIME IN SECONDS |      | WAKFLD |      | PASS NO = |      | 2989   |      |        |

75°

76.5°  
IN LAT

78°

Figure 3-11. H<sup>+</sup> - O<sup>+</sup> phase shift details.

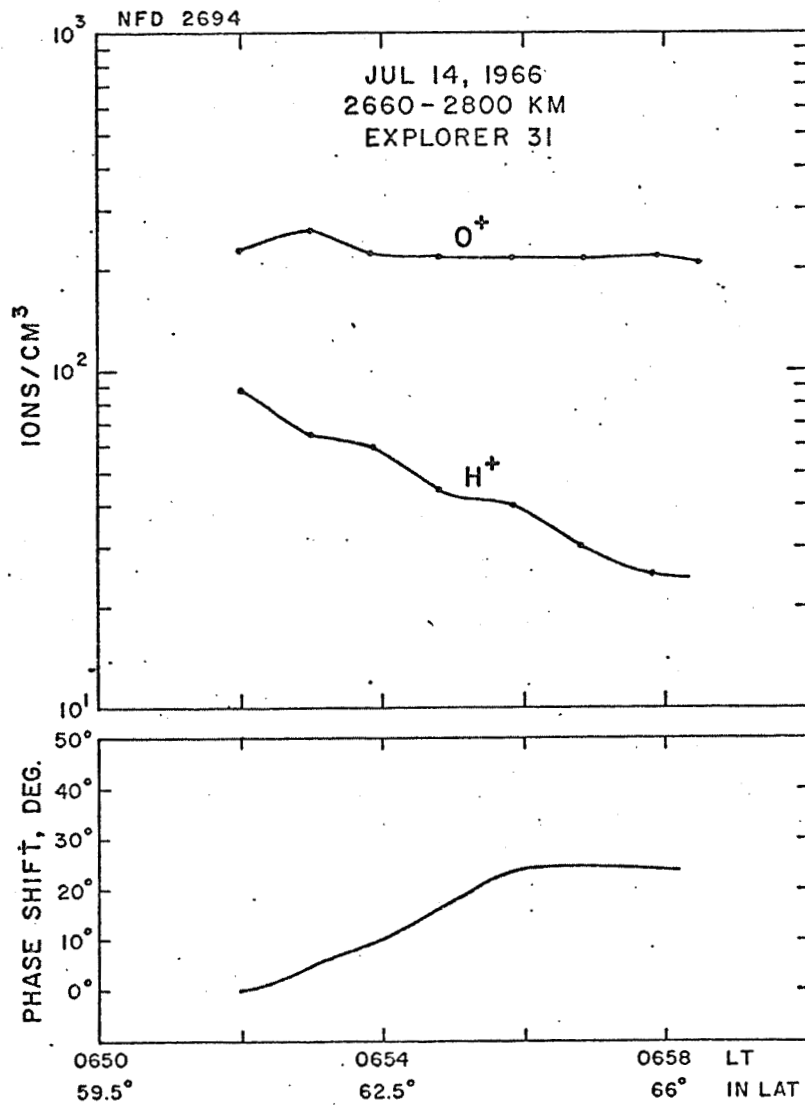


Figure 3-12. Phase shift onset.

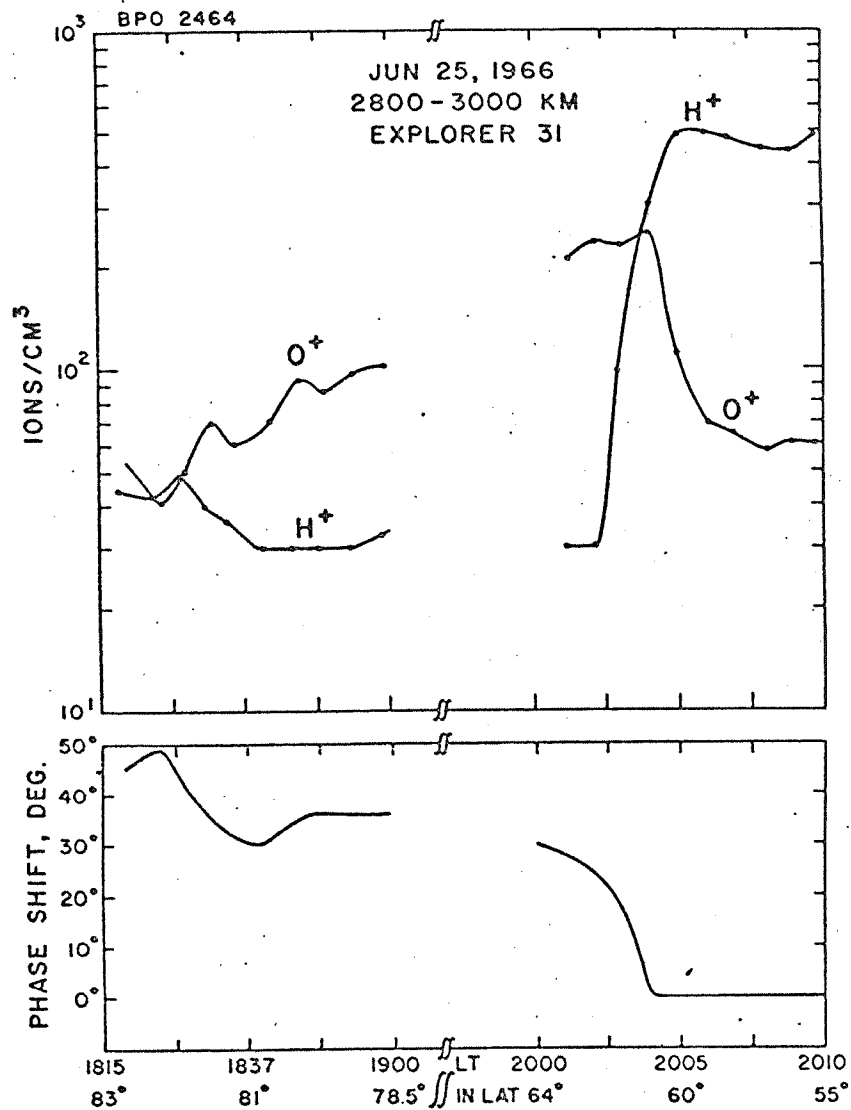


Figure 3-13. Ion composition and  $H^+$  phase shift. The plasmopause appears at  $61^\circ$  invariant latitude with increases of the  $H^+$  flow speed to  $4 \text{ km sec}^{-1}$ . The escape flow continues within the polar cap, reaching  $7 \text{ km sec}^{-1}$  at  $83^\circ$ .

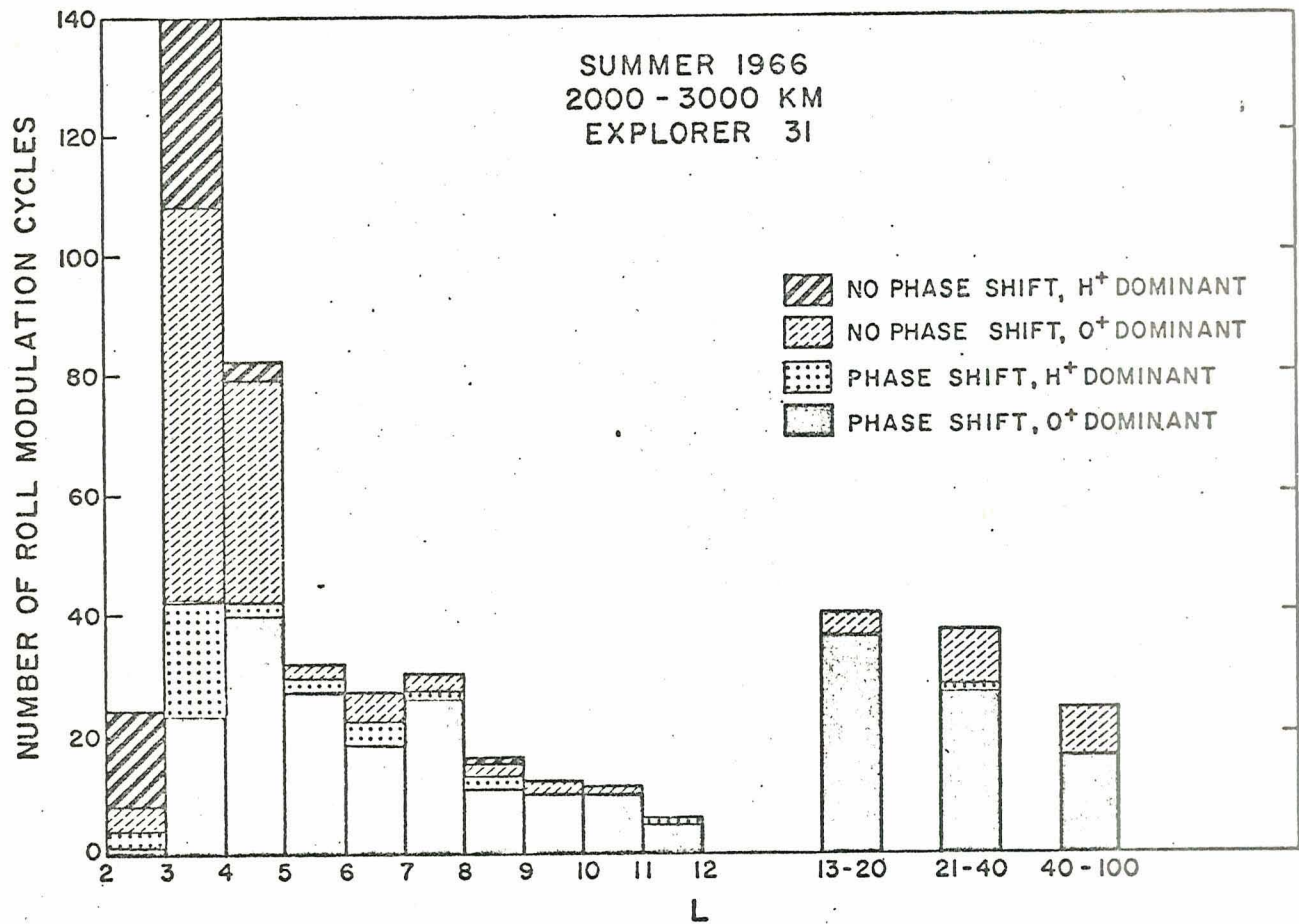


Figure 3-14. Phase shift histogram.

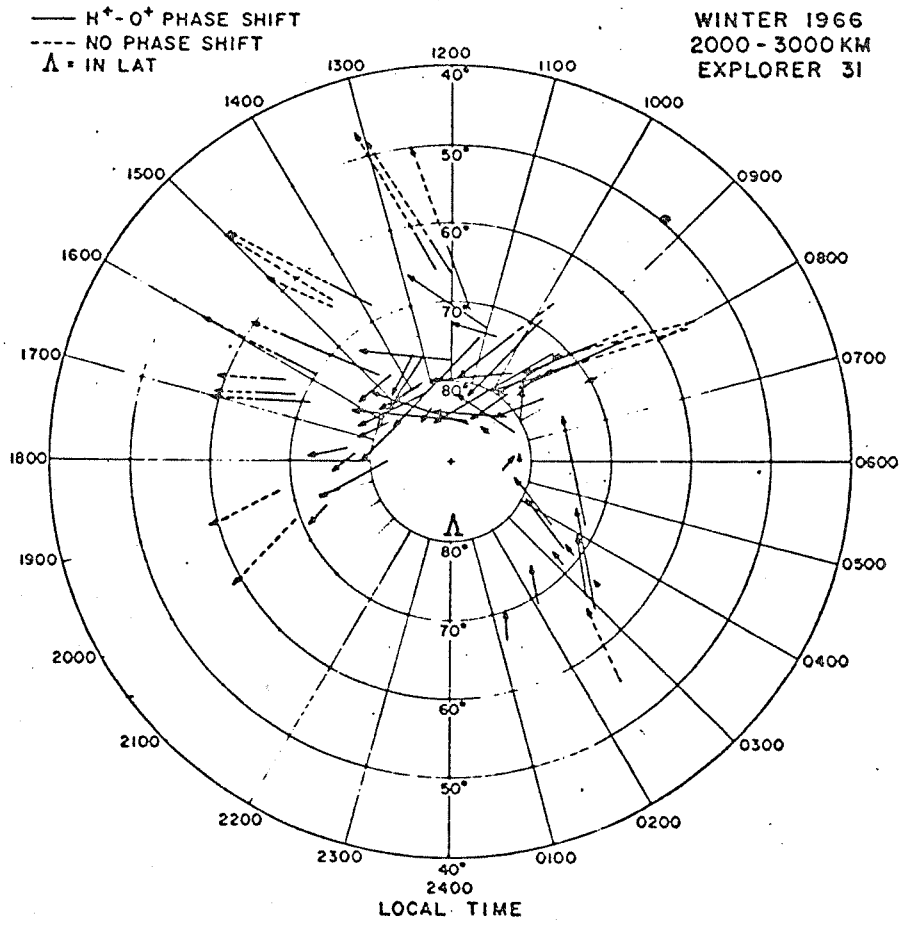


Figure 3-15. Observations of polar wind flow in the winter polar cap.



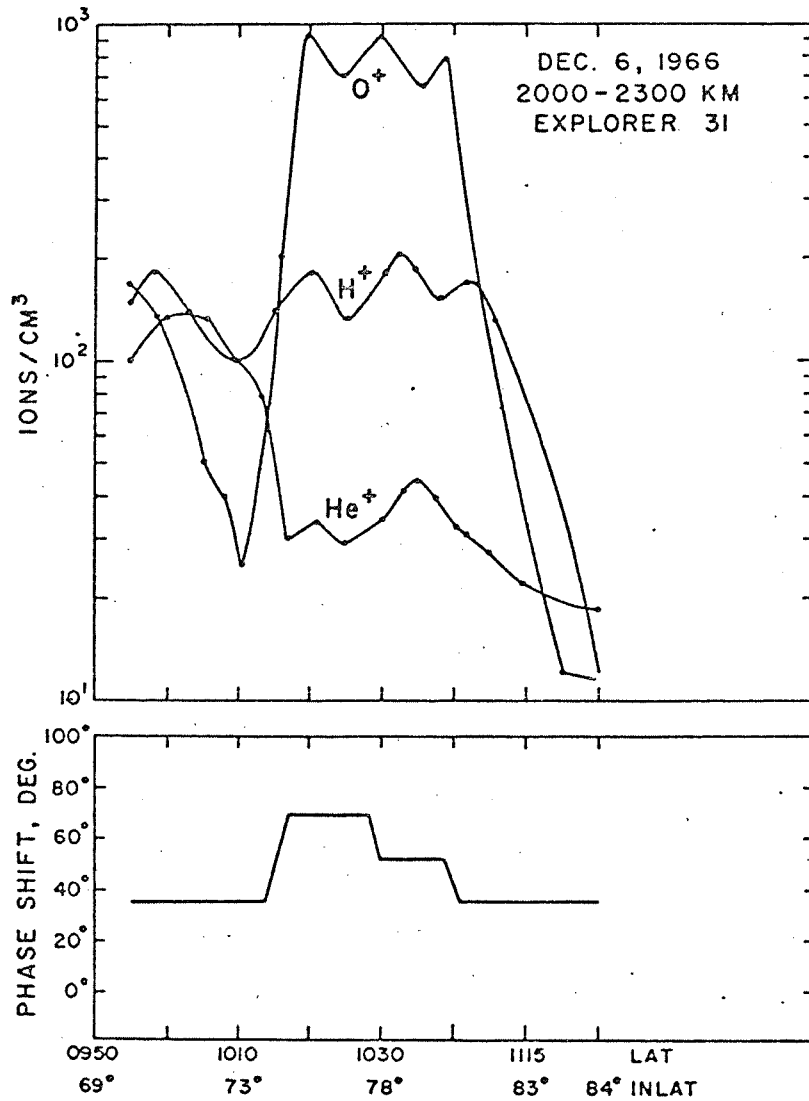


Figure 3-16. Ion composition and H<sup>+</sup> flow velocity measured in the polar cusp. A peak H<sup>+</sup> speed of 19 km sec<sup>-1</sup> was noted.

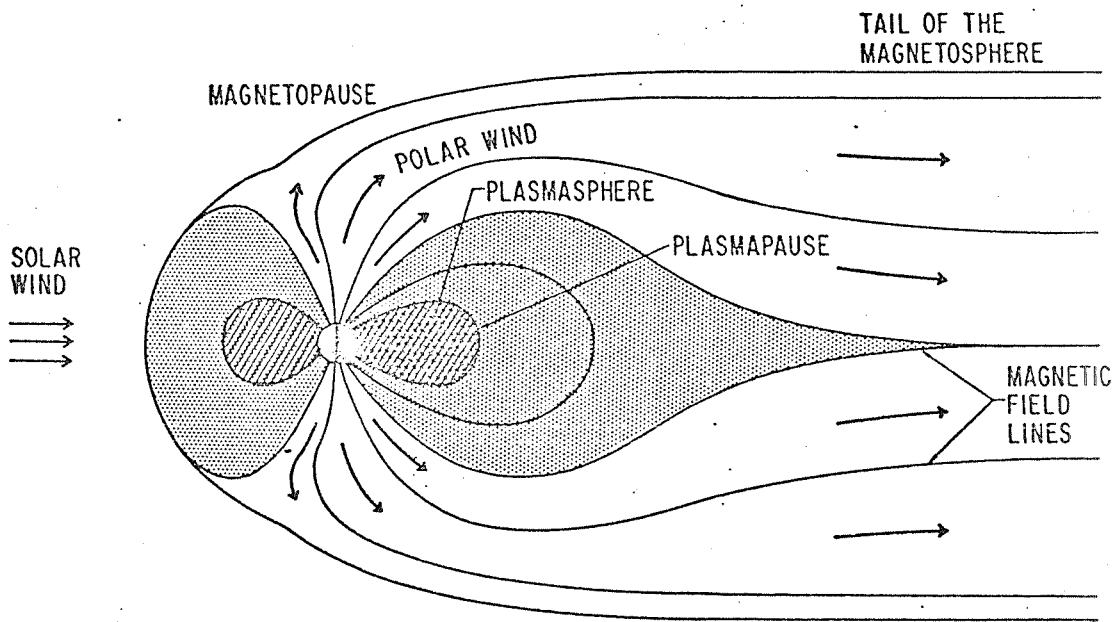


Figure 3-17. The different regions of the magnetosphere. In the plasmasphere field lines are closed and, to a large extent, co-rotate with the earth. At very high latitudes the field lines are open to the tail of the magnetosphere. Between the plasmopause and open regions field lines are closed, but convect around the earth.

## REFERENCES

1. Hoffman, J. H., "Composition measurements of the topside ionosphere," *Science*, 155, 322, 1967
2. Banks, P. M., and Holzer, T. E., "The polar wind," *Journal of Geophysical Research*, 73, 6846, 1968
3. Nelms, G. L., Private communication, 1968
4. Lohr, L., Private communication, 1967
5. Donley, J. L., et al., "Comparison of results of Explorer XXXI direct measurement probes," *Proceedings of IEEE*, 57, 1078, 1969
6. Knudsen, W. C., "Evaluation and demonstration of the use of retarding potential analyzers for measuring several ionospheric quantities," *Journal of Geophysical Research*, 71, 4669, 1966
7. Krankowsky, D., Kasprzak, W. T., and Nier, A. O., "Mass spectrometric studies of the composition of the lower thermosphere during summer 1967," *Journal of Geophysical Research*, 73, 7291, 1968
8. Hanson, W. B., and Ortenburger, I. W., "The coupling between the protonosphere and the normal F-region," *Journal of Geophysical Research*, 66, 1425, 1961
9. Banks, P. M., "Dynamic behavior of the polar topside ionosphere;" presented at the NATO Advanced Study Institute, Espedaleu, Norway, April, 1971

## SECTION 4

### INSTRUMENT DESCRIPTION

#### 4.1 GENERAL

The instrument on the Explorer XXXI satellite designed to measure the composition of the earth's ionosphere is a 1-1/2-inch radius, 60-degree sector field magnetic mass spectrometer. It scans the mass range from 1 to 20 amu and has a sensitivity to  $H^+$  ions of the order of one ion per  $cm^3$  and to  $O^+$  ions of the order of ten ions per  $cm^3$ .

The complete package weighs 11-3/4 pounds and measures 10-1/2 x 8-1/2 x 6-1/2 inches. It consumes 1.6 watts of power. Electronics modules are housed below the base plate. Figures 4-1 through 4-4 illustrate the physical features of the instrument.

Figure 4-1 shows the entrance aperture (to the left), the magnet and the electron multiplier housing of the mass spectrometer. The entrance aperture which looks out the side of the satellite normal to the spin axis, consists of a 3-inch diameter, fine-wire screen followed by an annular metal plate. The screen is commandable to either spacecraft ground potential or -6V with respect to the satellite skin potential. Field strength in the gap of the magnet in the analyzer section is 2200 gauss. A Bendix magnetic electron multiplier, M308, serves as the ion detector.

#### 4.2 OPERATION

The instrument operates as follows: The entire analyzer tube and magnet are swept through a negative high voltage range (-4000 to -150 volts) causing ambient ions from the region in the vicinity of the entrance aperture to be drawn into the instrument and to be separated into their constituent species by the magnetic analyzer. The sweep period for the mass range 1 to 20 amu is 3 seconds. An electron multiplier and a solid state logarithmic electrometer amplifier, which has a current sensitivity range of  $2 \times 10^{-12}$  to  $1 \times 10^{-6}$  amperes for a voltage output range of 0 to 5 volts, comprise the output circuitry. Rise and fall times of the amplifier are of the order of 5 ms. The output voltage of the log amplifier plus a monitor of the high voltage sweep are telemetered to Earth. An internal calibrator in the log amplifier supplies currents of  $10^{-11}$ ,  $10^{-9}$ ,  $10^{-7}$  ampere to the amplifier input once each 100 seconds of operation. The resulting output voltages are used to generate constants in the calibration equation that relates volts, the output of the log amplifier, to input current. These constants are updated at each calibration cycle.

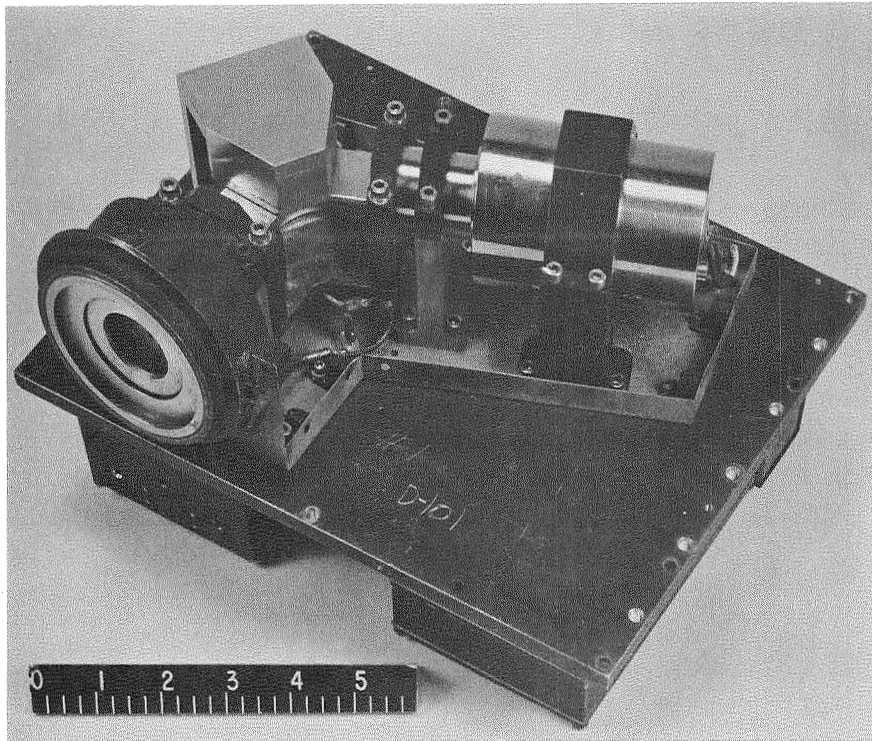


Figure 4-1. Ion Mass Spectrometer

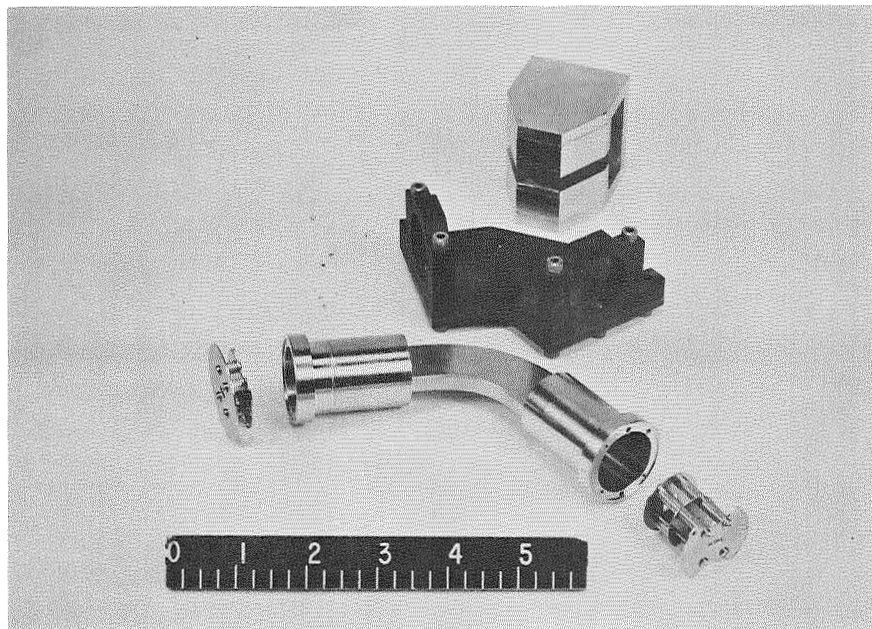


Figure 4-2. Analyzer Assembly

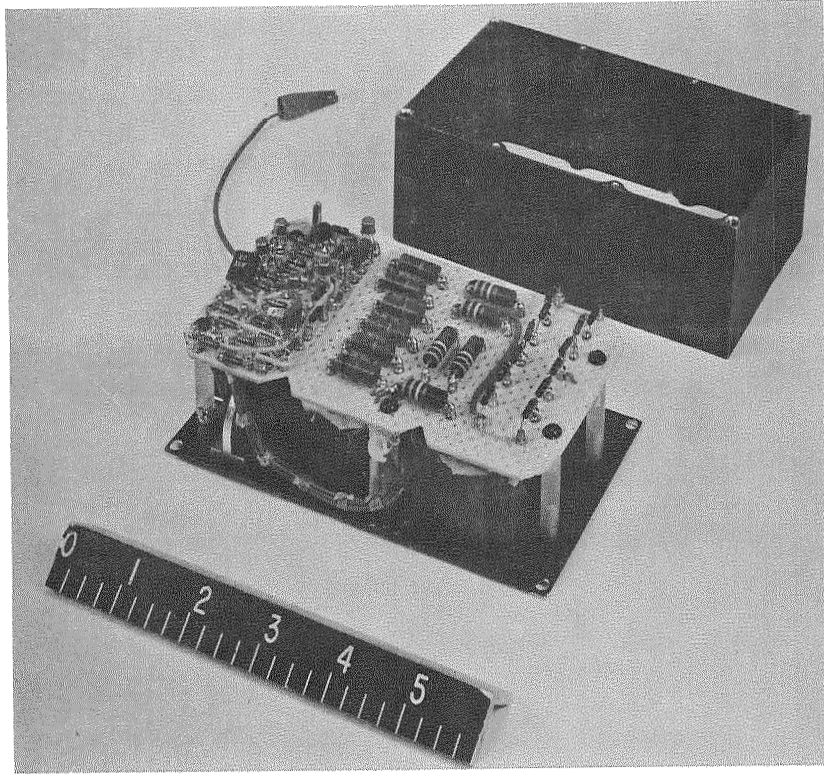


Figure 4-3. Electronics Unit

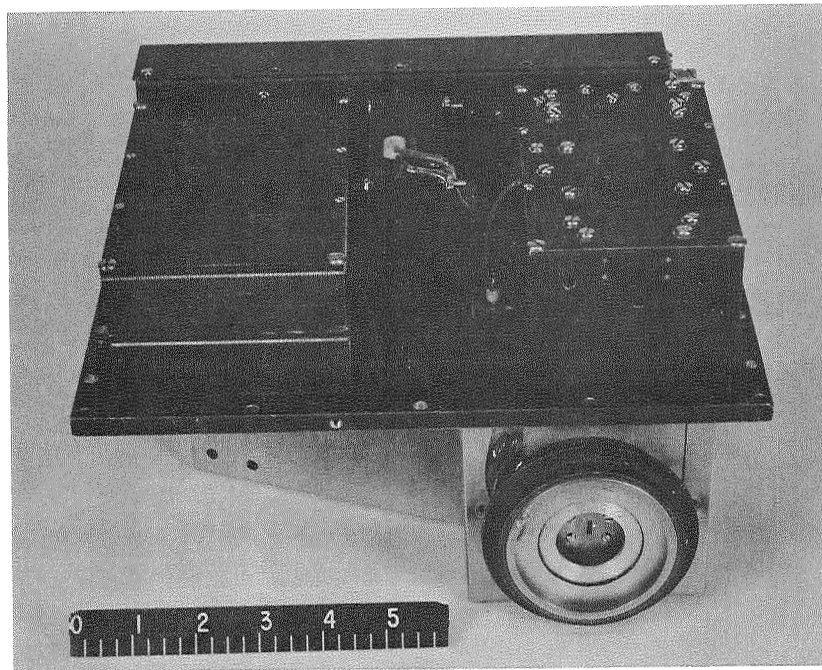


Figure 4-4. Bottom View

Figure 4-5 shows a sample analog telemetry record with the sweep voltage on the top channel and the mass spectrum below. The position of a peak in the spectrum determines the ion species being measured. The amplitude of the peak is proportional to the logarithm of the ion current detected by the electron multiplier for the ion species. This ion current is a function of the concentration of that species in the vicinity of the entrance aperture of the mass spectrometer. However, the concentration of ions in this region is dependent on the satellite attitude, velocity, and potential and has a complex relation to the ambient ion concentration. An in-flight calibration, which is described below, is necessary to obtain absolute ion concentrations.

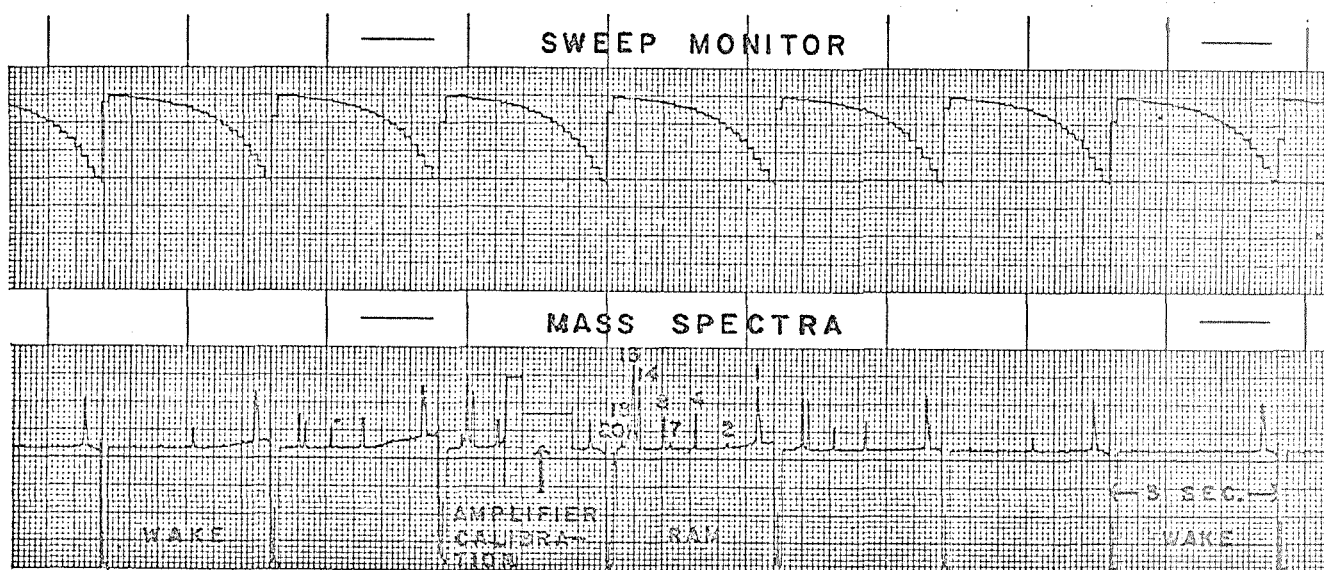


Figure 4-5. Portion of analog telemeter record. Upper channel is sweep monitor. Lower channel is mass spectrum. Downward blips are markers to show recharge of high-voltage sweep circuit. Ion peaks are labeled in atomic mass units. Internal 3-point amplifier calibration operates every 100 seconds.

Shown in Figure 4-5 are typical data of a pass taken near perigee (500 km), with peaks due to ions of hydrogen (1 amu), deuterium (2 amu), helium (4 amu), doubly charged nitrogen (7 amu), doubly charged oxygen (8 amu), nitrogen (14 amu), oxygen (16 amu), water vapor or  $O^{18}$  (18 amu) and neon (20 amu) are observed in the ram position. For the first two months of life of the satellite the mass 18 peak was principally due to water vapor. The amplitude gradually decreased while the roll modulation (described below) increased leaving a residual peak due to  $O^{18}$ , the  $O^{18}/O^{16}$  ratio being about that of normal ground level oxygen. Occasionally a mass 15 peak from  $N^{15}$  is observed, the  $N^{15}/N^{14}$  ratio



being about that of normal nitrogen. The mass 8 peak may also consist partly of  $\text{He}_2^+$ , but at low altitudes, where  $\text{O}^+$  is the dominant constituent it is likely that the mass 8 peak consists mainly of  $\text{O}^{++}$ , formed by photoionization of  $\text{O}^+$ . At the wake position, only peaks at mass 1 and 4 amu are visible and these are reduced in amplitude from the ram condition.

At altitudes near apogee (3000 km) at mid to low latitudes the mass spectra show only peaks at 1, 2, 4 and occasionally 8 amu. These are identified as hydrogen (1 amu), deuterium (2 amu), helium (4 amu) and  $\text{He}_2^+$  (8 amu). In this region no  $\text{O}^+$  is observed so the mass 8 peak is probably due to the  $\text{He}_2^+$  ion.

The satellite is oriented so that its spin axis is maintained normal to the orbital plane (a cartwheel orbit). Thus, the mass spectrometer entrance aperture on the side of the satellite alternately points along the satellite velocity vector, the ram condition, and opposite to it, the wake condition.

Since the satellite is traveling at a speed greater than the mean velocity of the ambient hydrogen ion, the ram and wake conditions are exhibited as a roll modulation in the ion peak amplitudes. The satellite spin period varies from 7 to 12 sweep periods. Figure 4-5 shows one roll modulation cycle. The mass 1 peak is relatively constant while the heavy ion peaks (mass 14, 16, 18) are absent in nearly half of the spectra.

Figure 4-6 is a plot of the peak amplitudes of successive mass spectra as a function of time. The roll modulation is quite evident and it should be noted that its amplitude is a strong function of ion mass. For  $\text{H}^+$  it is about 1 order of magnitude; for  $\text{He}^+$  2-1/2 orders of magnitude; and for  $\text{O}^+$  more than 5 orders of magnitude.

#### 4.3 CALIBRATION

An ion mass spectrometer measures relative abundances of the ions it samples from the ionosphere but can be calibrated, as is described below, to give absolute ion concentrations. Several factors cause the spectrometer to discriminate against ions of heavy mass. First, the instrument scans the mass spectrum by varying the ion accelerating voltage in an exponential manner from 4000 to 150 volts. Low mass ions are measured near the high voltage end of the sweep where the instrument has a higher transmission factor than at the low voltage/high mass end. This phenomenon is known as the voltage effect. Second, light mass ions, being more mobile than heavy mass ions, are collected from a larger volume. Hence, a larger light mass ion current is measured for equal concentrations of light and heavy mass ions. Third, the roll modulation amplitude has been shown above to be a strong function of ion mass. It is therefore most practical to measure the ion abundance ratios only in the ram condition, when the sensitivity for each constituent is a maximum.





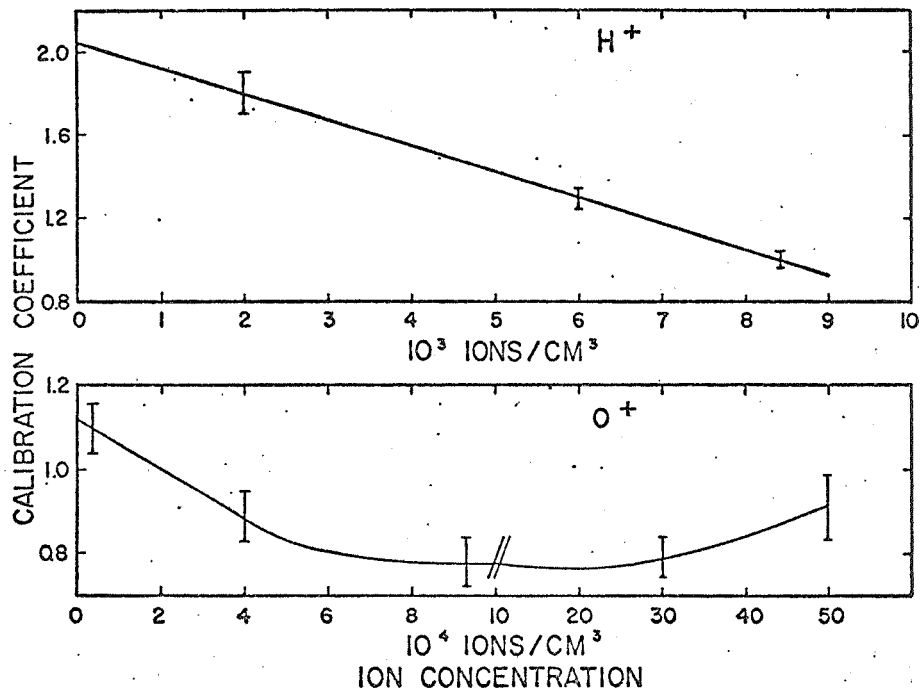


Figure 4-7. Calibration coefficients. Ratio of Alouette electron density to H<sup>+</sup> and O<sup>+</sup> concentration. Note scale change in abscissa of O<sup>+</sup> curve.

Data are plotted over a range of concentration from  $9 \times 10^3$  (the maximum H<sup>+</sup> concentration that has been observed) to  $1 \times 10^3$  ions per cm<sup>3</sup>. A linear relationship is seen to exist. The fact that the calibration coefficient is not constant may be due to the variation in plasma sheath thickness around the satellite as the ion concentration changes. Thus, a direct calibration of the absolute sensitivity of the mass spectrometer to H<sup>+</sup> was obtained. Next, a similar calibration was made for O<sup>+</sup> using ionospheric regions that were greater than 90 percent O<sup>+</sup>. In this case the calibration for H<sup>+</sup> was incorporated into the calculation. The concentration for the O<sup>+</sup> calibration, as shown in Figure 4-7, ranges from  $5 \times 10^5$  to  $1 \times 10^2$  ions per cm<sup>3</sup>. A linear relationship exists at lower concentrations but a saturation effect and reversal set in above  $10^5$ . At low concentrations (below  $10^3$ ) the sheath has little effect on the sampling volume and hence the calibration coefficient. The absolute sensitivity of the mass spectrometer for the other ions was then obtained by interpolation from these data. Obviously, the accuracy of sensitivity of the minor constituents is less than that for H<sup>+</sup> and O<sup>+</sup>, but since the concentrations of these species generally lie below  $10^3$  (except for N<sup>+</sup> whose mass and mobility is close to O<sup>+</sup>) the calibration coefficients are almost constants. Most of the passes used for this calibration procedure were different from the passes selected for comparison with the other experiments on Explorer XXXI, the results of which are presented in the paper entitled "Comparison of Results of Explorer XXXI Direct Measurement Probes" (Donley, Brace, Hoffman, Wrenn, 1969). Hence, the comparisons in the latter paper show the degree of agreement between the results obtained by applying the calibrations discussed here and the results obtained by the other experiments in this program. This agreement is generally to about 10 percent.

A typical example of the result of this in-flight calibration procedure is shown in Figure 4-8. The absolute concentration of each ion species is plotted against satellite altitude. The Alouette II topside sounder data for the same pass is also shown. Agreement between the total ion concentration,  $N_i$ , as determined by the sum of the individual ion species concentrations, and the electron density is of the order of 10 percent. In this pass the ion composition changes from 75%  $O^+$  at 1620 km to 66 percent  $H^+$  at 1170 km. Thus it can be seen that the mass spectrometer is capable of making absolute ion concentration measurements to the order of 10% when calibrated against simultaneous electron concentration data such as obtained from the topside sounder.

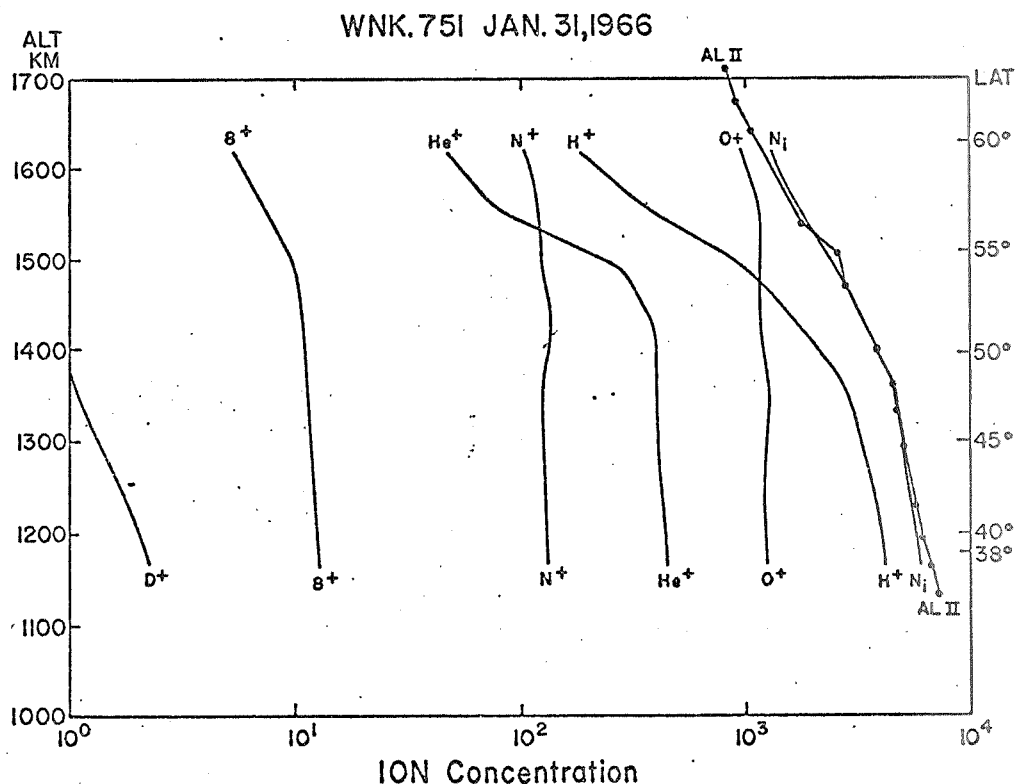


Figure 4-8. Comparison of ion data with Alouette II electron concentrations. Concentrations are plotted as a function of both altitude and latitude.

The mass spectrometer has a sensitivity to  $H^+$  ions of the order of 1 per  $cm^3$  and to  $O^+$  ions of 10 per  $cm^3$ . The Alouette II topside sounder data when analyzed by the standard method (Nelms and Lockwood, 1966) can give electron concentration data as low as several hundred electrons per  $cm^3$ . For concentrations below this level the beat frequency method due to Hagg (1967) must be employed. Since the mass spectrometer can also measure concentrations in this range, a comparison was made with the Alouette data for a high altitude pass, No. 209, that traversed the northern polar region.

The results are shown in Figure 4-9. This pass shows a region of highly variable ion concentration. The Alouette data are given as X's for the standard method of reduction and as O's for the Hagg data. Above a concentration of 500 ions per  $\text{cm}^3$  the agreement is to within 20 percent except at the extreme left in the figure (where one point differs by 30 percent and one by 40 percent) for both a predominantly  $\text{H}^+$  ionosphere, and for an  $\text{O}^+$  region near the center of Figure 4-9. For concentrations between 30 and 100 ions per  $\text{cm}^3$  at  $70^\circ$  to the left and again from  $85$  to  $90^\circ$ , regions where  $\text{He}^+$  is predominant, and to the right at  $80^\circ$  to  $75^\circ$  ( $\text{H}^+$  and  $\text{O}^+$  regions, highly structured) the agreement with the Hagg results is also to the order of 20 percent. Below 30 ions per  $\text{cm}^3$  the mass spectrometer data lies well below the Hagg results. In fact, in part of the region over the pole, the mass spectrometer shows no ions (less than one per  $\text{cm}^3$ ) while the Hagg method shows concentrations of 15 to 30 electron per  $\text{cm}^3$ . In this region the spacecraft potential has gone sufficiently positive, as determined by the ion trap on the satellite, to repel all ions from the satellite. Apparently it requires electron concentrations of the order of 30 per  $\text{cm}^3$  to sufficiently neutralize the spacecraft potential, made positive by photoemission, to allow the mass spectrometer to collect any ions at all from the region around the spacecraft. However, when this condition does exist, that the spacecraft potential is near zero (within 1 or 2 volts), the mass spectrometer results agree reasonably well with the topside sounder results down to a concentration of 30 ions per  $\text{cm}^3$  as shown by this example.

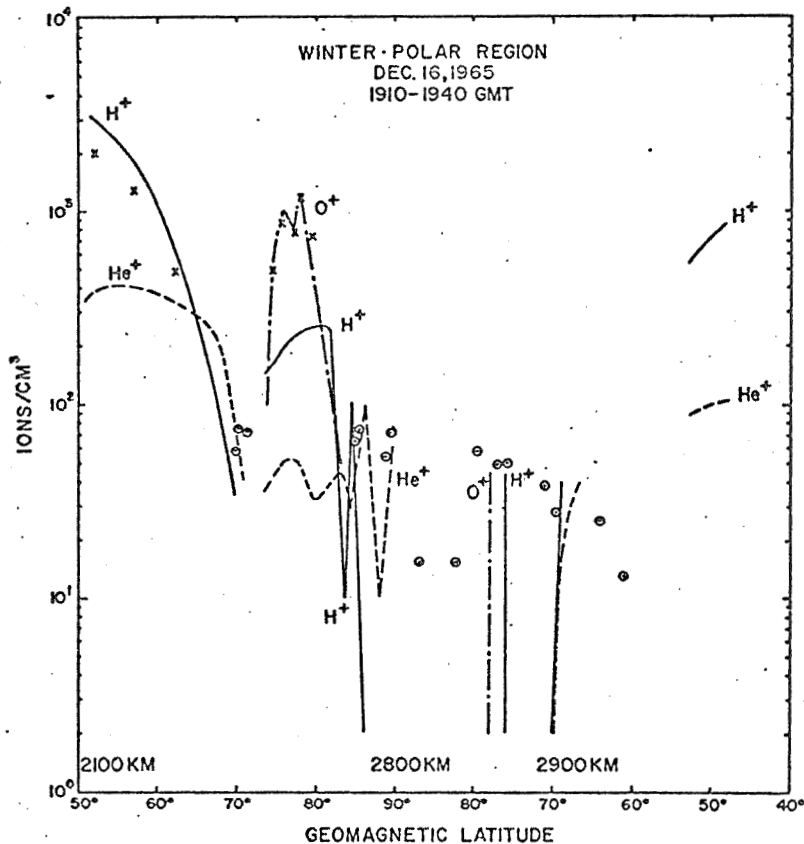


Figure 4-9. Comparison of mass spectrometer and Alouette II data.